

Comparative metabologenomics analysis of polar actinomycetes.






SOLDATOU, S., ELDJÁRN, G.H., RAMSAY, A., VAN DER HOOFT, J.J.J.,
HUGHES, A.H., ROGERS, S. and DUNCAN, K.R.

2021

© 2021 by the authors. Licensee MDPI, Basel, Switzerland.

Article

Comparative Metabologenomics Analysis of Polar Actinomycetes

Sylvia Soldatou ^{1,†} , Grímur Hjörleifsson Eldjárn ², Andrew Ramsay ², Justin J. J. van der Hooft ³ ,
Alison H. Hughes ¹ , Simon Rogers ²  and Katherine R. Duncan ^{1,*} 

¹ Strathclyde Institute of Pharmacy and Biomedical Sciences, University of Strathclyde, Glasgow G4 0RE, UK; s.soldatou@rgu.ac.uk (S.S.); a.hughes@strath.ac.uk (A.H.H.)

² School of Computing Science, University of Glasgow, Glasgow G12 8RZ, UK; 2332462H@student.gla.ac.uk (G.H.E.); andrew.ramsay@glasgow.ac.uk (A.R.); Simon.Rogers@glasgow.ac.uk (S.R.)

³ Bioinformatics Group, Wageningen University, 6708 PB Wageningen, The Netherlands; justin.vanderhooft@wur.nl

* Correspondence: katherine.duncan@strath.ac.uk

† Current address: School of Pharmacy and Life Sciences, Robert Gordon University, Aberdeen AB10 7GJ, UK.

Abstract: Biosynthetic and chemical datasets are the two major pillars for microbial drug discovery in the *omics* era. Despite the advancement of analysis tools and platforms for multi-strain metabolomics and genomics, linking these information sources remains a considerable bottleneck in strain prioritisation and natural product discovery. In this study, molecular networking of the 100 metabolite extracts derived from applying the OSMAC approach to 25 Polar bacterial strains, showed growth media specificity and potential chemical novelty was suggested. Moreover, the metabolite extracts were screened for antibacterial activity and promising selective bioactivity against drug-persistent pathogens such as *Klebsiella pneumoniae* and *Acinetobacter baumannii* was observed. Genome sequencing data were combined with metabolomics experiments in the recently developed computational approach, NPLinker, which was used to link BGC and molecular features to prioritise strains for further investigation based on biosynthetic and chemical information. Herein, we putatively identified the known metabolites ectoine and chlroramphenicol which, through NPLinker, were linked to their associated BGCs. The metabologenomics approach followed in this study can potentially be applied to any large microbial datasets for accelerating the discovery of new (bioactive) specialised metabolites.

Keywords: Actinobacteria; marine; Polar; genomics; metabolomics; specialised metabolites



Citation: Soldatou, S.; Eldjárn, G.H.; Ramsay, A.; van der Hooft, J.J.J.; Hughes, A.H.; Rogers, S.; Duncan, K.R. Comparative Metabologenomics Analysis of Polar Actinomycetes. *Mar. Drugs* **2021**, *19*, 103. <https://doi.org/10.3390/md19020103>

Academic Editor: Max Crüseemann

Received: 21 January 2021

Accepted: 8 February 2021

Published: 10 February 2021

Publisher's Note: MDPI stays neutral with regard to jurisdictional claims in published maps and institutional affiliations.



Copyright: © 2021 by the authors. Licensee MDPI, Basel, Switzerland. This article is an open access article distributed under the terms and conditions of the Creative Commons Attribution (CC BY) license (<https://creativecommons.org/licenses/by/4.0/>).

1. Introduction

More than 80 years after the first reported case of sulphonamide-resistant bacterial strains [1], antibiotic resistance is now a global threat to human health, projected to cause 10 million deaths annually by 2050 [2,3]. Historically, microorganisms have been a source of over 22,000 biologically active metabolites, including antibiotics, isolated from terrestrial and marine strains [4]. In particular, the order Actinomycetales (actinomycetes) has been shown to produce structurally diverse specialised metabolites which exhibit a wide range of biological activities. Indeed, more than 7000 metabolites have been isolated from the genus *Streptomyces* and approximately 3000 metabolites from the “rare” (due to their lower isolation frequency) actinomycete genera [5]. Actinomycetes have an average genome size of over 5 Mb. However, this number varies greatly between genomes which can reach up to 12 Mb in some *Streptomyces* species [6]. Actinomycetes dedicate 0.8–3.0 Mb of their whole genome to specialised metabolite production, which has been shown to result in 20–50 Biosynthetic Gene Clusters (BGCs) per strain [7]. A recent study of 21 rare marine actinomycetes isolated from temperate and sub-tropic marine environments unveiled

diverse and numerous BGCs, with *Actinomadura* spp. and *Nocardia* spp. containing 44 and 38 BGCs per strain, respectively. Interestingly, only three percent of the BGC families overlapped between the *Streptomyces* strains and the rare actinomycetes, suggesting an exciting resource for biosynthetic novelty [8]. Moreover, analysis of 119 genomes of the rare actinomycete genus *Salinispora* derived from various sub-tropic and tropic locations revealed 176 BGCs, of which only 24 were linked to their respective products [9], indicating a potential resource for novel metabolites.

Although actinomycetes from the (sub-)tropics have been extensively studied and shown to be a promising source of biological and chemical novelty, Actinobacteria isolated from Polar regions also show potential for affording new biologically active specialised metabolites. Actinobacteria accounted for 5% of the total microbial community present in Antarctic sediment samples as revealed by high-throughput 16S rRNA gene sequencing, with the *Salinibacterium* genus being amongst the most abundant [10]. In terms of isolating rare actinomycetes from Polar habitats, a study of ancient Antarctic and sub-Arctic sediment samples yielded 50 bacterial strains, of which 39 belonged to rare actinomycetes genera (*Microbacterium*, *Dietzia*, *Rhodococcus*, and *Pseudonocardia*) [11]. Regarding the chemical potential, molecular networking indicated rare actinomycetes from sub-Arctic and Antarctic sediments to be a rich source of metabolites [11,12]. Since 2001, a total of twenty-nine new metabolites have been isolated from Antarctic and sub-Arctic bacteria, with 13 being produced by marine actinomycetes [13]. For example, the rare actinomycete *Nocardia dassonvillei* BM-17 isolated from an Arctic sediment sample yielded a new phenazine derivative with significant antifungal and cytotoxic activity [14]. Two new α -pyrones were isolated from an Antarctic *Nocardiopsis* strain [15], whereas the seaweed-derived *Nocardiopsis* sp. 03N67 collected in the Arctic Ocean afforded a new diketopiperazine, cyclo-(L-Pro-L-Met), which showed promising anti-angiogenesis activity [16].

It is widely known that variations in cultivation parameters can induce the expression of so-called ‘silent’ BGCs, for which the biosynthetic enzymes have been identified but no natural product has been isolated from laboratory cultures [17]. Hence, changes in abiotic factors such as nutrient availability (carbon, nitrogen, trace-elements), temperature, salinity, and pH have been shown to influence the production of such ‘cryptic’ specialised metabolites. Moreover, the chemical profile of a microorganism can depend on the culture vessels, shaking conditions, and aeration, as well as on co-culturing techniques [18]. For example, when glucose was substituted for glycerol in the ISP2 growth medium, the liquid culture of *Streptomyces* sp. C34 isolated from the Atacama Desert, yielded ansamycin-type polyketides [19]. Furthermore, the marine-derived *Streptomyces* sp. CHQ-64 was found to produce new biologically active polyene-polyols and hybrid isoprenoid alkaloids when cultured under shaking, whereas static fermentation yielded only one new metabolite [20,21]. Therefore, the “One Strain Many Compounds” (OSMAC) approach [22] has been a successful addition in the microbial drug discovery pipeline

Mass spectrometry approaches are often used to compare multi-strain metabolomics. Molecular networking using the Global Natural Products Social Molecular Networking (GNPS) infrastructure [23] has been deemed a valuable tool in the discovery of new metabolites [24] as it provides rapid dereplication [25] and identification of unknown parent ions. Clarinoside, a new pentalogin from the plant *Mitracarpus scaber* Zucc [26], retimycin A, a non-ribosomal peptide from *Salinispora arenicola* [27], and deoxyphorbol ester derivatives from *Euphorbia dendroides* [28] are a few of the specialised metabolites discovered using MS-guided isolation based on the GNPS platform. Recently, further analysis tools have been implemented on the GNPS infrastructure, such as MS2LDA which provides fragmentation patterns of commonly co-occurring mass fragment peaks and/or neutral losses that often represent molecular substructures (Mass2Motifs) [29], and Network Annotation Propagation (NAP) [30] which improves in silico fragmentation of the input data. The MolNetEnhancer workflow was introduced to combine the outputs of the above-mentioned tools and add (putative) chemical class annotations to molecular families in the molecular network [31].

The sequencing of the first *Streptomyces* genome in 2002 [32] paved the way for the discovery of further microbial natural products based on genomic data. The continuous development of genome sequencing technology has led to a wealth of genomic data which has motivated the development of sophisticated mining tools that can augment the search and discovery of novel specialised metabolites [33,34]. Several of these [35] are publicly accessible, enabling thorough and targeted genome mining of complex bacterial genomes, including antiSMASH for the identification of secondary metabolites BGCs [36], ARTS for high-throughput screening of bacterial genomes in reference to antibiotic production [37], and BiG-SCAPE for clustering BGCs into Gene Cluster Families (GCFs) [38].

The linking of genome and metabolome mining outcomes to accelerate natural products discovery has shown great promise over the last decade, with several tools contributing to bridging the gap between BGCs and mass spectra [39]. Although the term “metabologenomics” was officially introduced in 2016 to describe correlations between BGCs and metabolites [40], research on this approach started earlier. A study of actinomycete strains in which their genomic data were linked with MS profiles, led to the identification of GCFs for the previously reported natural products desertomycins and oasamycins, for which the corresponding BGCs were unknown [41]. The authors were also able to isolate and characterise a new chlorinated metabolite, tambromycin, and correlate it with its BGC in 11 actinomycete strains using metabologenomics [40]. Another successful study used a combination of molecular networking and pattern-based genome mining approach from which arenicolide A was linked to an uncharacterised BGC (PKS28) and the new metabolite, retimycin A was identified, characterised and linked to the known NRPS40 pathway [27].

Herein, we introduce a novel unsupervised *-omics* integration method to link tandem mass spectrometry data to BGCs to accelerate the analysis of large microbial natural products datasets. NPlinker, a newly introduced software framework [42] was applied for the first time to bridge the large metabolomics and genomics datasets of marine Polar Actinobacteria. With the aid of the novel approach Rosetta, links between spectra and BGCs for chloramphenicol and ectoine were established. Molecular networking of the 100 metabolite extracts derived from applying the OSMAC approach, showed growth media specificity and potential chemical novelty was suggested. Moreover, the metabolite extracts were screened for antibacterial activity and promising selective bioactivity against drug-persistent pathogens such as *Klebsiella pneumoniae* and *Acinetobacter baumannii* was observed.

2. Results

2.1. Phylogenetic Analysis

Twenty-five strains, 14 Antarctic and 11 Arctic, were selected from a larger collection of Polar marine sediment bacteria mainly consisting of Actinobacteria [11], based on taxonomy, isolation location (depths ranging from 388 to 4730 m) and previously known metabolic profile of the strains. The selected strains belonged to seven rare actinomycete genera—*Pseudonocardia* (eight strains), *Micrococcus* (seven strains), *Rhodococcus* (three strains), *Microbacterium* (three strains), *Kocuria* (one strain), *Agrococcus* (one strain), *Dietzia* (one strain). This genus-level delineation was well supported with bootstrap values over 67% and all strains clade with their respective reference sequences. Additionally, one strain of the phylum Proteobacteria, belonging to the *Halomonas* genus, was included in the study (Figure 1, Table S1). In terms of core depth (Figure 1), the two *Agrococcus*, one *Kocuria* and the eight *Pseudonocardia* strains were only isolated from the deepest sediment cores at a depth greater than 4000 m, and the one *Halomonas* and the two *Microbacterium* strains were only isolated from core depths of 1000–4000 m, while no pattern was observed for the genera *Micrococcus* and *Rhodococcus*. Although these observations are interesting, larger strain numbers would be required to draw statistical conclusions.

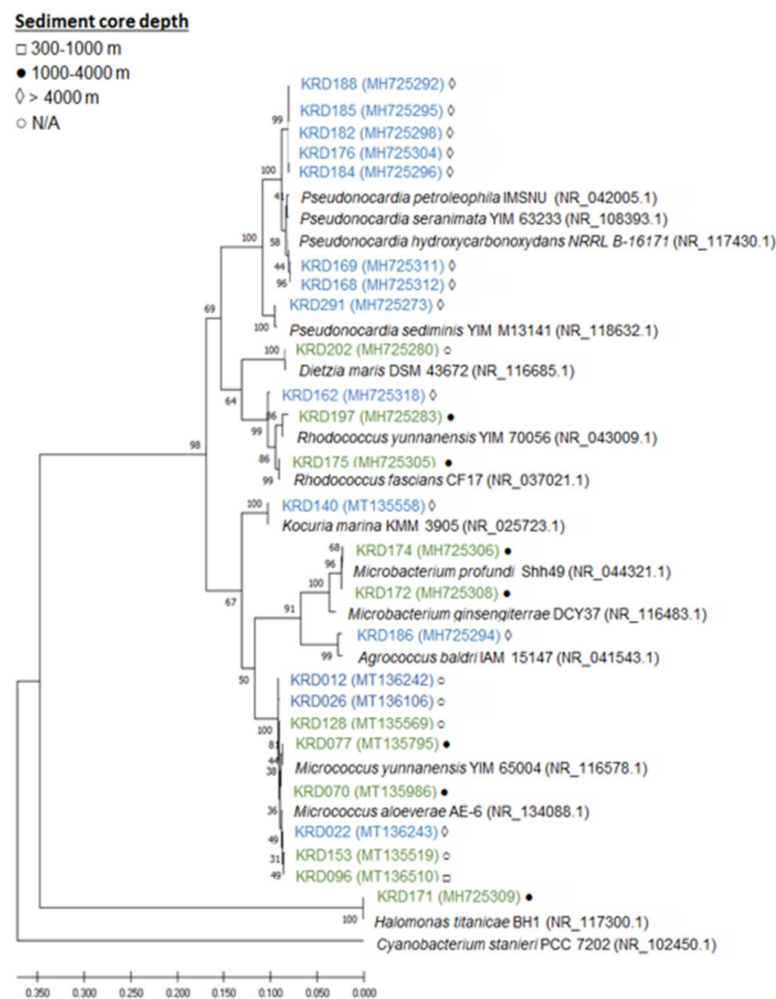


Figure 1. Maximum likelihood tree based on 16S rRNA gene sequences of 25 strains isolated from Antarctic (blue) and Arctic (green) sediment samples. Strain numbers are followed by a symbol indicating the depth at which the sediment samples were collected from: □ 300–1000 m, ● 1000–4000 m, ◇ > 4000 m and ○ N/A (information missing). The accession number is shown in brackets following the strain name.

2.2. Genome Mining

Genome assembly was carried out using SPAdes and due to the large numbers of contigs obtained, MeDuSa was utilised for genome scaffolding, using reference strains with >95% similarity based on 16S rRNA sequencing data (Table S2). No reference strains with >95% sequence similarity could be identified for the *Pseudonocardia* strains; therefore, they were eliminated from genome mining to avoid possible discrepancies.

Genome mining of the seventeen Polar rare Actinobacteria and the Proteobacteria (*Pseudonocardia* strains excluded) revealed a total of 133 BGCs including NRPS, PKS, terpene and RiPP classes. Interestingly, 37% of the total BGCs showed no homology to any BGC within the MiBIG database and a further 30% suggested homology ranging from 2% to 63% to known antibiotics. The biosynthetic diversity per strain is shown in the Circos diagram (Figure 2). The width of the bands indicates the number of BGCs within each Natural Product (NP) class which, as expected, is positively correlated to genome size. The lowest number of BGCs was observed for small genomes such as the *Micrococcus* (2.4–2.7 Mbp) and *Agrococcus* (3.1 Mbp) both of which had five BGCs, whereas the three *Rhodococcus* strains (5.4–6.7 Mbp) revealed the largest number (17–22) of BGCs. Moreover, strains belonging to the same genus showed BGCs of the same NP class (Table S3). The ectoine pathway was observed in almost all genomes except the *Kocuria* (KRD140) and the *Microbacterium*

(KRD174) strains. A similar pattern was observed for the terpene BGC which was present in the genome of all Polar isolates except the *Halomonas* strain (KRD171) (Table S3). The most abundant NP class was NRPSs which were not evenly distributed among all strains, as the smaller genomes such as *Micrococcus* and *Microbacterium* did not show any NRPS BGCs, although at least one NRPS-like fragment was identified in their genomes. On the other hand, larger genomes such as the *Rhodococcus* strains revealed a high number of NRPS BGCs (up to 10). Identification of siderophores based on bioinformatic analysis can often be challenging as many siderophores are produced through NRPS pathways, thus antiSMASH identifies them as NRPS and not siderophores [8,43]. Indeed, antiSMASH identified two NRPS clusters in one *Halomonas* strain (KRD 171) and one *Rhodococcus* strain (KRD 197) that have 53% and 63% gene homology to the serobactin and heterobactin siderophore pathways, respectively. Only 10 BGCs belonging to the PKS family were observed, of these, five were identified as Type I PKS, one Type II PKS, three Type III PKS, and one heterocyst glycolipid synthase-like PKS (hgIE-KS).

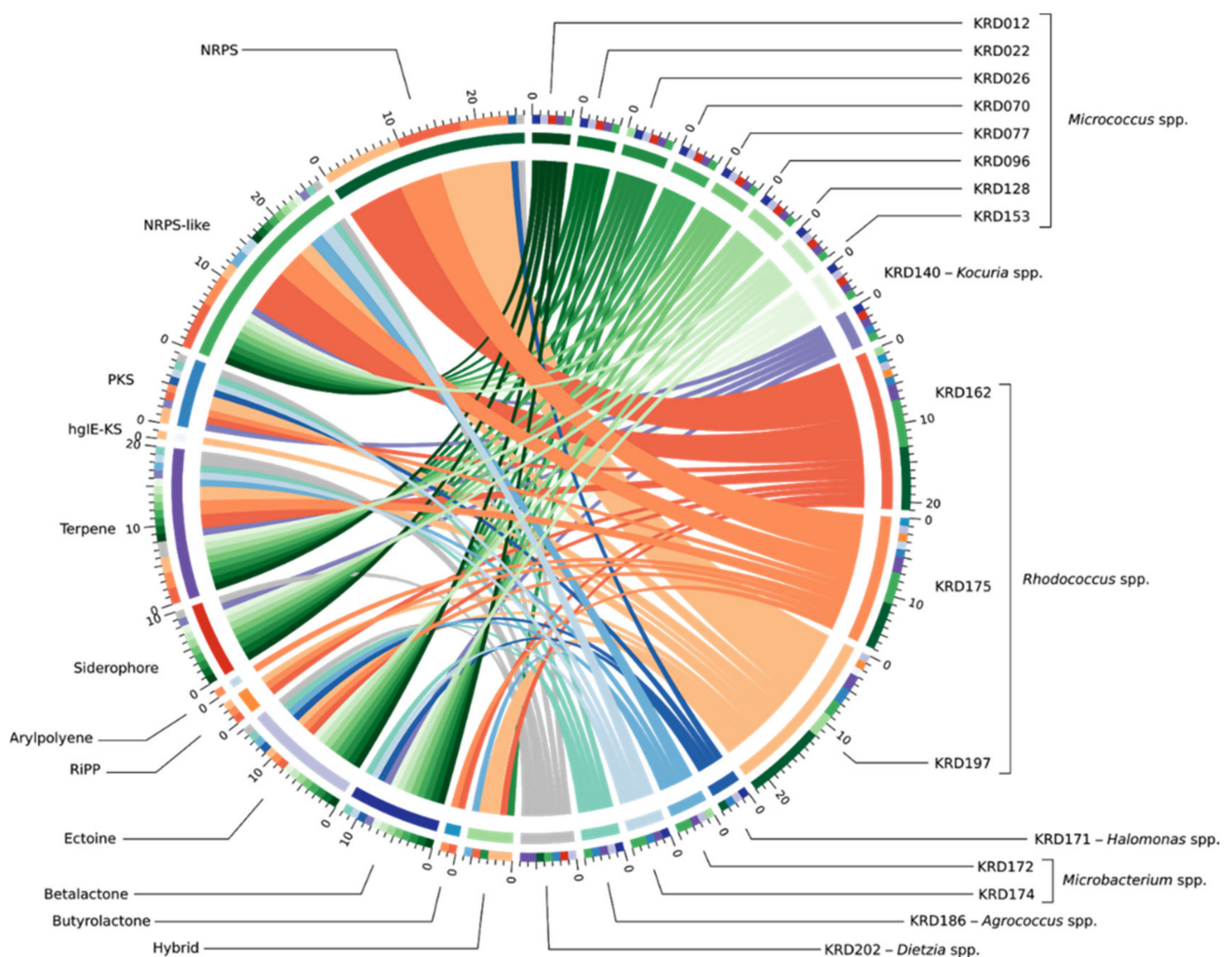


Figure 2. BGC diversity by NP class and strain taxonomy across 17 Polar strains. The band colour depicts taxonomy at the genus-level *Micrococcus* spp. (green), *Kocuria* sp. (purple), *Rhodococcus* spp. (orange), *Halomonas* sp. (dark blue), *Microbacterium* spp. (light blue), *Agrococcus* sp. (teal) and *Dietzia* sp. (grey). Each coloured band can be traced from the organism (right half of the circle) to the types of BGCs found in that genome (left half of the circle). The width of the band represents the number of BGCs of that NP class. The outer rings on the left of the diagram show the number of the BGC types found in each microbial genome. BGCs are colour coded based on the NP classification.

The BGCs of the 17 Polar strains were further analysed using BiG-SCAPE, which resulted in 80 GCFs, with 46% shown as singletons. As expected, there were BGCs present in strains belonging to the same genus, that clustered in the same GCF. For example, the ectoine BGCs present in the eight *Micrococcus* strains clustered in one GCF and the ectoine BGCs of the three *Rhodococcus* strains were represented as an additional GCF (green circles in Figure 3). The three *Rhodococcus* strains had a terpene BGC which showed low homology (6%) to SF2575 BGC from the soil-derived *Streptomyces* sp. SF2575 [44] (blue circle in Figure 3). Although the homology with the known biosynthetic pathway is low, the fact that it is shared by all three BGCs from the different *Rhodococcus* strains, implies that the strains may produce the same or similar metabolite(s) to the tetracycline antibiotic SF2575 [45]. Additionally, the three *Rhodococcus* strains (KRD12, KRD175, KRD197) showed an NRPS BGC that shows low homology (11%) to the chloramphenicol BGC from *Streptomyces venezuelae* ATCC 10712 [46]. Interestingly, only the gene clusters of KRD175 and KRD162 were grouped in the same family, whereas the corresponding BGC of KRD197 was shown as a singleton (red circles in Figure 3) even running BiG-SCAPE with a high cut off (0.7). Further investigation of the antiSMASH data showed that the predicted metabolites for the NRPS genes of interest could be cyclic lipopeptides, which often exhibit antibiotic properties [47].

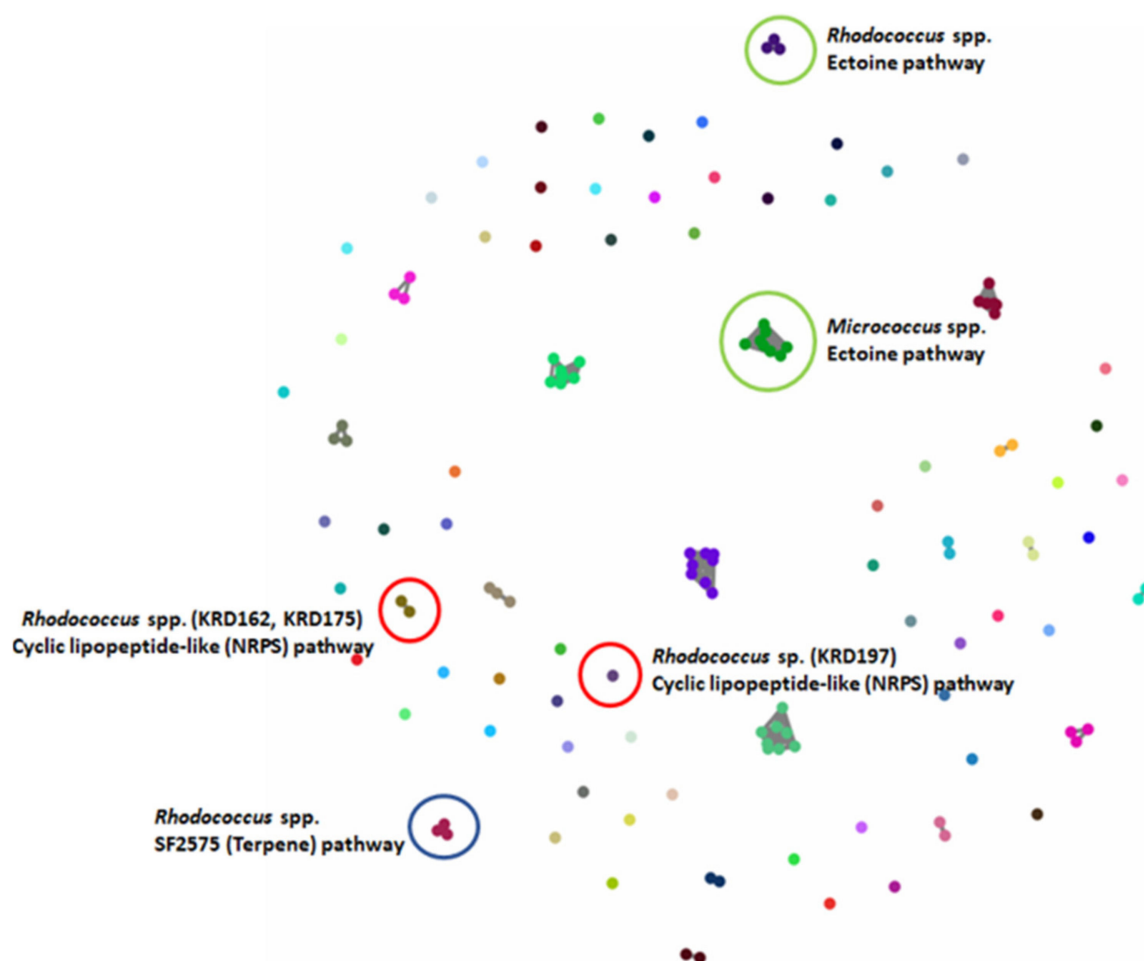


Figure 3. BiG-SCAPE analysis of 17 strains. The 133 BGCs; 53 NRPS/NRPS-like, 20 Terpene, 10 PKS, 3 RiPP and 47 others (including BGCs such as ectoine, siderophore, betalactone) were clustered in 80 GCFs. Examples of GCFs of interest are highlighted in coloured circles; red represents the *Rhodococcus* spp. NRPS BGC corresponding to a potentially new cyclic lipopeptide, green represents the ectoine pathway found in all strains (here highlighted for the *Micrococcus* and *Microbacterium* spp.) and blue the terpene BGC found in all three *Rhodococcus* strains with low homology to the known antibiotic SF2575.

2.3. Antibacterial Activity and Parent Ion Distribution

Culturing all strains in four growth media resulted in 100 metabolite extracts, of which 72% exhibited activity against six pathogenic bacteria (*Escherichia coli*, *Staphylococcus aureus*, *Klebsiella pneumoniae*, *Acinetobacter baumannii*, *Pseudomonas aeruginosa* and *Enterococcus faecalis*) known as the “ESKAPE” pathogens [48]. Specifically, 39% of the biologically active strains (28% of the total number) showed antibacterial activity against only one pathogen. The same percentage of active extracts inhibited the growth of one or more pathogens under only one cultivation condition. The inhibition zones ranged from 0.1 to 2.1 cm (Table S4). Most of the bacterial metabolite extracts were active against *S. aureus* with the *Pseudonocardia* strain KRD185 showing the largest inhibition zone (2.1 cm). Moreover, the 10-fold diluted TSB extract of strain KRD185 showed promising antibacterial activity against *K. pneumoniae* (0.9 cm) and *A. baumannii* (1.5 cm), whereas the A1M1 and 10-fold diluted TSB extracts of *Rhodococcus* strain KRD175 were selectively active against *K. pneumoniae* (Table S4). The occurrence of parent ions in relation to the bioactive extract is shown in Figure 4 where Hinton diagrams are illustrating the number of parent ions produced only by each strain (strain specific), as well as shared between two strains (Figure 4A). Strains belonging to the same genus shared the highest number of produced parent ions, which of course varies between the genera. For example, within the *Micrococcus* genus, strains KRD022 and KRD026 share the highest number of parent ions (649 in total), whereas strains KRD128 and KRD096 share only 287 parent ions. For the *Pseudonocardia* spp. isolates, there is a wide variation in the number of shared parent ions (163–632), where strain KRD176 shares 632 ions with KRD196 and only 163 with KRD291. Variations ranging from 104 to 649 shared parent ions also occurred between strains of different genera, as expected. The *Microbacterium* sp. strain KRD174 shared 104 and 123 parent ions with *Micrococcus* sp. KRD096 and *Pseudonocardia* sp. KRD291, respectively, representing the lowest number of shared ions. On the other hand, the *Rhodococcus* strain KRD175 showed the largest number of shared parent ions (649) with strain KRD022 of the *Micrococcus* genus. The sole *Kocuria* sp. isolate, KRD140, shared only 199 parent ions with *Pseudonocardia* strain KRD176, but shared more than 400 ions with three *Pseudonocardia* strains (KRD182, KRD185, KRD188). Amongst the *Pseudonocardia* strains, KRD182 showed the highest number of shared parent ions with *Micrococcus* spp. (356–607 parent ions), and *Rhodococcus* strains (465–612 parent ions). The Hinton diagram in Figure 4B demonstrates the number of parent ions produced by strains under each growth condition (white box), as well as the number of specific parent ions per strain grown under each growth condition (purple box) and the observed bioactivity (black outline). The 10-fold diluted TSB metabolite extract of KRD185 (*Pseudonocardia* sp.) had the highest bioactivity, with a zone of inhibition of 2.1 cm, and it produced the highest number of total (803) and unique (29) parent ions in that growth condition when compared to the rest of the studied isolates. Although the *Micrococcus* strain KRD022 produced the highest numbers of parent ions in ISP2 (819) and A1M1 (864) media, it did not exhibit any biological activity against the pathogenic bacteria. These two examples indicate that bioactivity is not necessarily related to the highest number of produced metabolites (parent ions).

2.4. Molecular Networking

A molecular network of all 100 microbial metabolite extracts (25 strains cultured in four media), in addition to the media and solvent blanks, consisted of 3107 parent ions (nodes). There were 721 nodes that were excluded from the data analysis as they corresponded to parent ions present in the media and solvent blanks. Of the total number of parent ions produced (i.e., not present in the blanks, 2386), 414 of these nodes were singletons indicating that their fragmentation pattern did not correlate with that of any other parent ion, suggesting chemical novelty within the dataset. After ions in the media controls were excluded, 23% (549) of ions were produced by strains grown in all four media. A further 65% (1551) of ions were produced in more than one medium (i.e., not media specific). Interestingly, the percentage of nodes which were media-specific was almost

constant across ISP2 (8.3%), ISP3 (8.8%), and 10-fold diluted TSB (8.0%) media, whereas 6.3% of the produced ions were present in the metabolite extracts derived from A1M1 medium. The MolNetEnhancer workflow showed 38 (putative) chemical classes annotated in the molecular network (Figure 5B and Figure S2). Almost 71% of the produced ions did not match any chemical classification which implies chemical novelty and is in accordance with the low number of library hits generated by the GNPS molecular network. Fatty acyls, and benzene and substituted derivatives represented 4% and 5% of the produced ions, whereas prenol lipids covered 6% of the chemical classes identified in the network.

2.5. Computational Pattern Matching

A recently introduced software framework, NPLinker, was utilised to suggest links between spectra of interest and their corresponding GCFs and therefore BGCs [42]. Initially, analysis was carried out using the standardised strain correlation scoring method which yielded potential MF-GCF links based upon correlating strain presence and absence. This approach greatly narrowed the space of links requiring investigation. Further analysis of the suggested links based on biosynthetic knowledge allowed the BGCs to be identified that were likely to be most relevant to the metabolite of interest. Specifically, the GNPS infrastructure allows parent ion clustering into molecular families and comparison of observed spectra with GNPS embedded libraries. Simultaneously, BGCs were clustered into GCFs via BiG-SCAPE. The generated MFs and GCFs were then uploaded to NPLinker where potential MF-GCF links were ranked based on two scoring functions; standardised strain correlation scoring and the here introduced, novel approach named Rosetta scoring (Figure 6A).

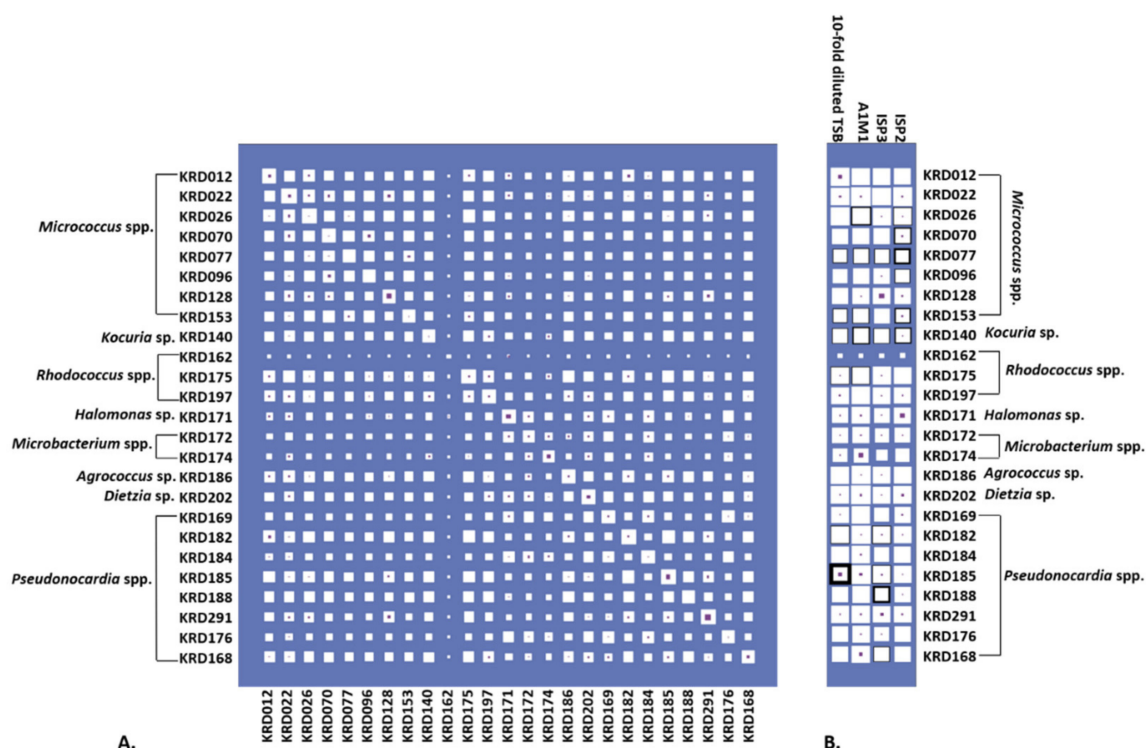


Figure 4. (A) Hinton diagram showing the number of parent ions (proportional to the size of white box) produced by each strain (max. 1041, min. 543 parent ions) and shared by each pair of strains (max. 670, min. 104 parent ions). Number of parent ions specific to that strain (or pair) are proportional to the size of the inner purple box. (B) Hinton diagram showing the number of parent ions by strain across each media (white box). Parent ions specific to only that strain-medium are also shown (purple box). The thickness of black box outline corresponds to the number of ESKAPE pathogens bioactivity was observed against (ranging from 1 to 6). For example, the bacterial metabolite extract for KRD185 in diluted TSB was found to be bioactive against all six pathogens, but no bioactivity was observed when the same strain was cultured in any of the other tested media.

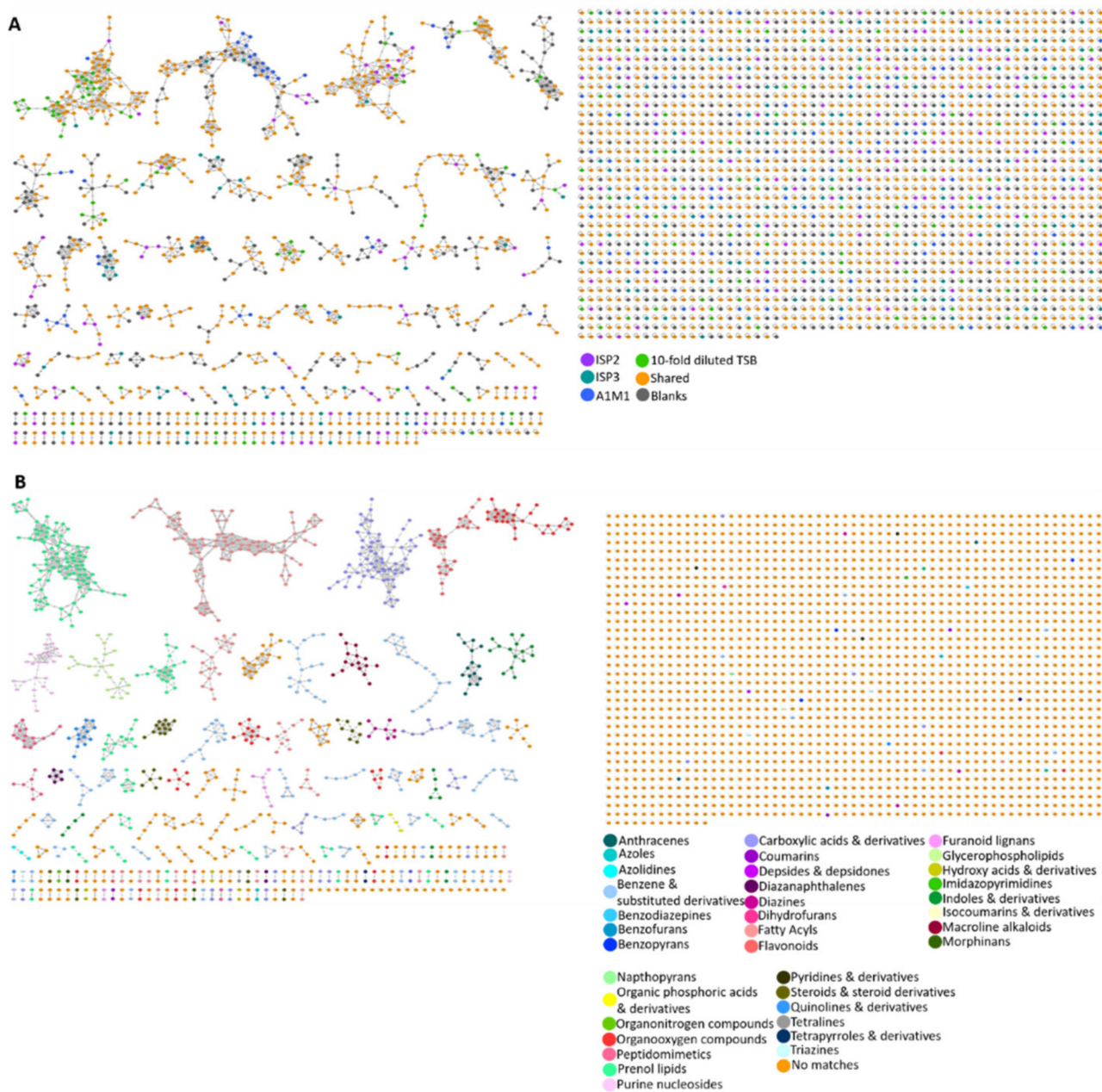


Figure 5. (A) Molecular network of 3107 parent ions produced by 25 strains cultured in four media and those found in media and solvent blanks. Nodes are colour coded based on media: ISP2, ISP3, A1M1 and 10-fold diluted TSB. Grey nodes represent media components, whereas orange nodes represent parent ions that are found in more than one different medium. (B) Nodes are colour coded based on 36 chemical class terms annotated using MolNetEnhancer workflow. Orange nodes represent parent ions that had no matches with any chemical class.

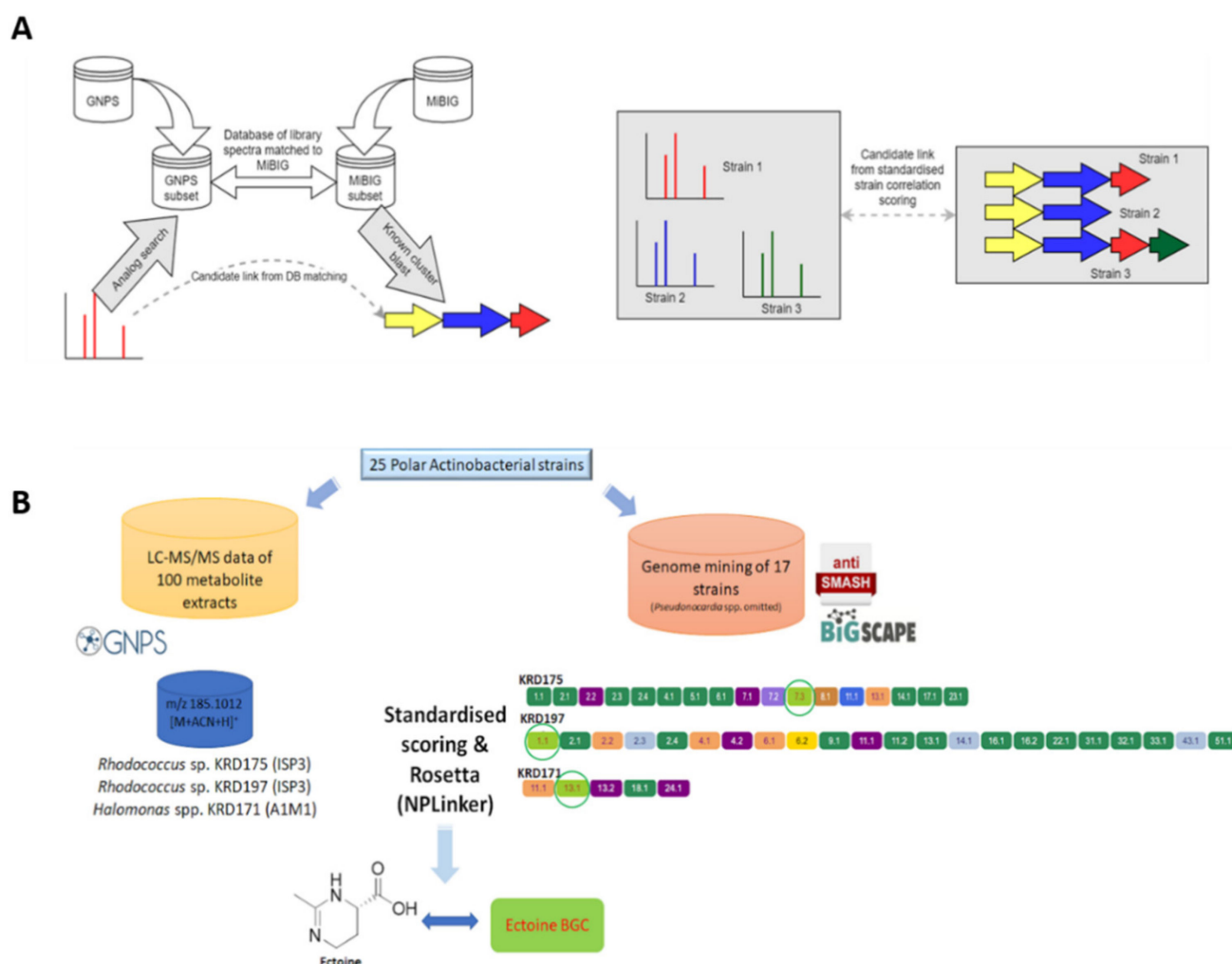


Figure 6. (A) Molecular families (MFs) are created through molecular networking using the GNPS infrastructure and parent ions of interest are identified through dereplication using GNPS embedded libraries and the Rosetta tool. Genome mining data (antiSMASH) of the Polar strains were clustered in GCFs using BiG-SCAPE. The GNPS (MFs) and BiG-SCAPE (GCFs) outputs are then analysed with NPLinker to rank potential MF-GCF links using two scoring functions (standardised strain correlation linking and Rosetta scoring). (B) The ectoine metabolite produced by two *Rhodococcus* spp. (KRD175 and KRD197) when cultured in ISP3 and one *Halomonas* sp. (KRD171) cultured in A1M1 was linked with its corresponding ectoine BGC via NPLinker.

2.5.1. Computational Pattern Matching Using the Standardised Strain Correlation Scoring Method

The parent ion (m/z 547.3815) produced by *Microbacterium* sp. KRD174 cultured in A1M1 showed spectral similarity to the GNPS spectrum CCMSLIB00000569369 suggesting it was an antimycin-related metabolite. Through NPLinker, it was shown that this metabolite could potentially be linked with the NRPS-like, betalactone, t3PKS and terpene BGCs (KRD174). Although the standardised strain correlation score for all links was high (2.7–4, with 4 being the maximum value observed in the dataset), when this information was combined with the fact that antimycins are produced by an NRPS/PKS hybrid [49], it was hypothesised that the betalactone and terpene BGCs were less likely to be involved in the biosynthesis of the metabolite of interest. Of course, further validation studies are required to confirm the responsible BGC. Similarly, another metabolite (m/z 521.3294) showed similarity with GNPS spectrum CCMSLIB00004710288 for conglobatin (MIBiG ID: BGC0001215), suggested that it could potentially be structurally related to the known macrolide conglobatin originally isolated from the antibiotic-producing *Streptomyces con-*

globatus [50]. The metabolite of interest was produced by two *Micrococcus* strains, KRR022 and KRD026 (diluted TSB medium), in addition to *Rhodococcus* sp. KRD175 (diluted TSB medium) and two *Pseudonocardia* strains KRD184 and KRD291 (ISP2 medium). Using the standardised strain correlation scoring method, the spectrum was potentially linked with 14 GCFs; two from *Micrococcus* sp. (KRD026) and 12 from *Rhodococcus* sp. (KRD175). However, the highest standardised strain correlation linking score (2.1) was observed for the hybrid BGC arylpolyene-NRPS (KRD026) as well as for the NRPS, NRPS-like, arylpolyene and butyrolactone BGCs (KRD175). Considering that conglobatin biosynthesis is governed by an NRPS/PKS BGC [51], the arylpolyene-NRPS BGCs are most likely to be involved in the biosynthesis, but further studies would be required to validate this. These examples demonstrate that using spectral library matches with the standardised scoring method included within NPLinker can narrow down possible MF-GCF links and thus enable a more focused downstream analysis.

2.5.2. Computational Pattern Matching Using Standardised Strain Correlation Scoring and the Rosetta Method

To further investigate the potential links between the genomics and metabolomics datasets of the Polar strains, an additional filter layer was added into NPLinker which allowed the use of the standardised strain correlation scoring method and the Rosetta hit list simultaneously. This approach led to linking spectrum ID 219769 (m/z 185.1012), putatively identified as ectoine ($[M + CAN + H]^+$ adduct), via Rosetta, with the ectoine BGC in two *Rhodococcus* sp. (KRD175, KRD197) and *Halomonas* sp. (KRD171) strains. Interestingly, when using only the standardised scoring the same spectrum was linked to 40 GCFs. However, applying the additional Rosetta scoring method narrowed it down to two GCFs (Figure 6B). Moreover, Rosetta identified that spectrum ID 111427 (m/z 380.2794) could be structurally related to the known antibiotic chloramphenicol, originally isolated from *Streptomyces venezuelae* [52]. The parent ion of interest was present in the metabolite extracts of *Rhodococcus* sp. KRD175 and *Micrococcus* sp. KRD128 and was linked with the NRPS BGC (KRD175) which showed homology to the chloramphenicol BGC. It is important to note that the Rosetta scoring approach is limited by the number of MiBIG BGCs for which experimental spectra are available. Due to the relatively low number of publicly available spectra of microbial metabolites [53], the combined filtering approach (standardised score and Rosetta) could only identify links for ectoine and chloramphenicol to their corresponding BGCs. It must be pointed out that the Rosetta hits were a result of matching single MS fragments to publicly available MS/MS datasets (Table S5), hence the aforementioned metabolites could be only putatively identified. However, this workflow clearly shows the promise of the implemented method for analysing large genomics and metabolomics datasets.

3. Discussion

Over the years, it has been shown that the Arctic and Antarctic marine environment host a vast variety of Actinobacteria with great potential for producing novel chemistry with a wide range of biological activities [11–13]. Bioprospecting for new specialised metabolites from Polar strains has greatly improved by the advancement of publicly available tools for untargeted metabolomics [23] and genome mining [54], which are continuously under development to meet the rapidly evolving field of microbial natural products discovery. One of the main challenges of genome mining is the quality of the genome assembly and annotation which can affect the outcome of the analysis [55,56]. A large number of contigs in the genome assembly can lead to BGCs, especially PKS-I and NRPS, to be broken across pieces and not being identified by available software and tools. A great example of such issue was demonstrated by Baltz who showed that draft genomes containing large NRPS/PKS-I genes were incorrectly assembled due to being largely fragmented which resulted in overestimation of such BGCs by antiSMASH 3.0 [57]. However, since then, new updated versions of antiSMASH have been released in which the location of the gene cluster close to the contig edge is flagged. Moreover, the need

for closed genomes is of paramount importance for accurate and reliable genome mining. However, long-read technologies are often required to achieve this, which comes with greater expense and their own drawbacks such as high error frequencies and reliability [58]. A recent study of nine Actinobacterial species, including three *Pseudonocardia* strains used short-read (Illumina MiSeq) and long-read (Oxford Nanopore MinION) sequencing technologies to analyse BGC fragmentation. The authors found that the MinION-based genome assemblies increased the sensitivity related to BGC annotation and reduced the number of fragmented BGCs. [56]. In this present study we omitted the *Pseudonocardia* strains from the genomic analysis due to lack of reference strains for genome scaffolding. Genome mining of the 17 non-*Pseudonocardia* strains revealed a wide diversity of BGCs with most of them having low homology to known BGCs which suggests biosynthetic and chemical novelty. Terpene BGCs were present in almost every genome, which was not surprising as recent studies have revealed a wide distribution of terpene synthases in bacteria which has led to the development of a new hidden Markov model for terpene synthases identification in bacterial genomes [58,59]. As expected, the number and variety of BGCs increased for larger genome sizes such as the *Rhodococcus* strains. However, it was unexpected to notice that smaller genomes such as *Micrococcus*, *Halomonas* and *Kocuria* were lacking PKS and NRPS BGCs as actinomycetes are known to produce metabolites encoded by those pathways [60,61]. A similar observation was made by Schorn et al. when studying rare marine actinomycetes [8]. Although small genomes might not look as promising from a natural products discovery perspective, it does not necessarily mean that they are not worth further investigation. The sponge-associated *Micrococcus* sp. was reported to produce a new antibacterial xanthone named microluside A [62] and marine *Halomonas* strains have yielded new antibacterial and cytotoxic metabolites named loihichelins A–F and aminophenoxazinones, respectively [63,64].

To further explore and investigate the observed BGCs in our Polar strains, analysis showed the ectoine BGC present in all genomes; this is known to be ubiquitous as the metabolite aids survival under extreme osmotic stress [65]. Moreover, the terpene BGC with high homology (66%) to a known carotenoid BGC was present in all *Micrococcus* strains and clustered in the same GCF. Carotenoids are terpenoids produced by all photosynthetic organisms and some non-phototrophic organisms, and have several applications as food colorants, feed supplements, nutraceuticals, and pharmaceuticals [66]. Terpene BGCs with homology (>37%) to the isorenieratene BGC were observed in the *Rhodococcus* strains and were clustered in the same GCF. Actinobacteria, and particularly *Streptomyces* spp., often bear isorenieratene BGCs in their genome that are usually silent, and there have been only a few cases in which these BGCs have been activated [67,68]. Furthermore, the genomic data of the three strains belonging to the genus *Rhodococcus* suggest the presence of NRPS BGCs which could potentially encode for cyclic lipopeptides. Such metabolites are of great importance in drug discovery with the example of daptomycin, originally isolated from the soil-derived *Streptomyces roseosporus* [69], which has been approved by the FDA as an antibacterial agent against Gram positive pathogens [70].

For over 30% of the BGCs within our dataset, the most similar known cluster encoded for an antibiotic. Of this, almost half showed low homology (<10%) with known BGCs. This is an exciting finding suggesting that the rare actinomycete strains derived from Polar marine sediments can potentially be a fruitful source of novel chemistry. It is worth noting that extracting metabolites from culture broth in organic solvents was proven to be a more effective and reliable method to assess biological activity (disc diffusion assay) than an agar plug assay [71]. Although genome mining of the *Rhodococcus* spp. showed promising potential for producing metabolites, the bioassay data did not fully support this. As only strain KRD175 exhibited moderate but selective activity against *K. pneumoniae*. This could be because the BGCs encoding for antibiotics remained silent or the biologically active compounds were produced in low amounts that were not sufficient to inhibit the growth of the pathogens. Moreover, the bacterial metabolite extracts mostly inhibited the growth of *S. aureus*, whereas only a few showed inhibitory effects against *K. pneumoniae* and *A.*

baumannii, which are two of the most drug-persistent pathogenic bacteria [72,73]. To the best of our knowledge, there are only a few published reports on the inhibitory effects of microbial specialised metabolites on *A. baumannii* [74–76] but none on *K. pneumoniae*; and therefore, the Polar strains with such activity show promise to combat these pathogens.

Linking genomic and metabolomics datasets of actinomycete strains for specialised metabolite discovery has been introduced only recently [41]. However, there is increased interest in the scientific community to further explore this niche research field by generating automated methods for correlating these complex datasets and ranking promising MF-GCF links for further investigation. Targeted linking and automated approaches for accelerating drug discovery have been reviewed [39,53]. Recently, metabolomic and genomic data of 72 isolates belonging to the rare actinomycete genus *Planomonospora* were analysed using publicly available tools to link specialised metabolites to their corresponding BGCs [77]. The authors were able to manually pair siomycin congeners to a RiPP BGC and a new salinichelin-like metabolite to the known BGC encoding for erythrochelin. In the present study, the newly developed software, NPLinker, was used to link our experimental datasets and prioritise strains for further chemical and biosynthetic investigation. The filtering approaches that were implemented (standardised strain correlation score and Rosetta) established links for ectoine and chloramphenicol to their corresponding BGCs but were not yet sufficient to link the potentially new identified metabolites (antimycins-like and conglobatin-like compounds) to GCFs as publicly available spectra of microbial metabolites are almost non-existent and remain mostly hidden in supplemental figures in literature. Van Santen et al. [78], among others, discussed the need for data sharing within the scientific community which will allow the field of natural products to catch up with data-centric approaches used in other research fields and further flourish. It is worth pointing out that limiting number of Rosetta hits obtained within this metabolomics dataset is indicative of the potential novel chemistry of the Polar strains which is further supported by the large number of nodes that could not be annotated to specific chemical classes. However, our findings agree with a recent literature review which reported only 29 new metabolites isolated from Antarctic and Arctic bacteria, of which 13 have been discovered from marine actinomycetes [13]. A future direction for NPLinker could be the integration of bioassay data along with metabolomics and genomics datasets, as previously suggested by others [79], which will give the opportunity to users to explore possible MF-GCF links based on bioactivity and target the BGCs and therefore the metabolite(s) responsible for the biological effect.

4. Materials and Methods

4.1. Phylogenetic Analysis

Twenty-four rare actinomycete strains and a marine strain of the phylum *Proteobacteria* (Table S1) were previously isolated and taxonomically identified (through 16S rRNA gene sequencing) from the Antarctic and sub-Arctic sediment core collection from two separate studies in conjunction with the Scottish Association for Marine Sciences [11,12]. These strains were selected based on taxonomy and isolation location. Using the 16S rRNA gene sequences, a maximum likelihood (ML) phylogenetic tree was constructed (Kimura 2-parameter model, 1000 bootstraps) using Mega 7 (v 7.0.26) (<https://www.megasoftware.net/> (accessed on 9 November 2020)) [80,81] with visualisation and annotation using FigTree (v 1.4.3) (<http://tree.bio.ed.ac.uk/software/figtree> (accessed on 9 November 2020)). The GenBank accession numbers for the 16S rRNA gene sequences are the following: MT135519 (KRD153), MT135569 (KRD128), MT135795 (KR077), MT135986 (KRD070), MT136106 (KRD026), MT136242 (KRD012), MT136243 (KRD022), MT136510 (KRD096). The remaining strains were deposited in GenBank as mentioned in [11].

4.2. Fermentation and Metabolite Extraction

All twenty-five strains were pre-cultured (5 mL, 28 °C, 160 rpm for 7 days) in ISP2 medium [82], ISP3 medium [82] A1M1 medium [27] and 10-fold diluted TSB medium

(BD™) prepared in distilled water. Instant ocean (18 g/L) was added in each of them. Each culture [ISP2/ISP3/A1M1/10-fold dil. TSB medium (50 mL) with activated HP-20 resin (Sigma) (2.5 g)] was inoculated (5% *v/v* pre-culture) and fermented (14 days, 28 °C, 160 rpm). The culture was then centrifuged (4000 rpm, 20 min), the supernatant removed, and the cell/resin pellet lyophilised until dry (Thermo Savant MicroModulyo, Thermo Fisher Scientific, Waltham, MA, USA). The lyophilised cell/resin pellet was extracted twice with ethyl acetate (Fisher Scientific, Loughborough, UK, reagent grade) (20 mL, 100 rpm, 25 °C). The extracts were combined, dried (under N₂), the weight recorded and stored (4 °C).

4.3. Bioactivity Disc Diffusion Assay

Cultures in TSB (BD™) were prepared for *Escherichia coli*, *Staphylococcus aureus*, *Klebsiella pneumoniae*, *Acinetobacter baumannii*, and *Pseudomonas aeruginosa*, whereas cultures in LB [peptone 10 g/L, yeast extract 5g/L, sodium chloride 5 g/L] (5 mL, 30 °C, 1200 rpm, 12 h) were prepared for *Enterococcus faecalis*. Nutrient agar (NA, 5 mL, ThermoFisher Scientific) was inoculated with 0.1 mg/mL of the pathogen and was poured onto NA Petri plates (10 mL). The ethyl acetate metabolite extracts were re-dissolved in ethyl acetate at a concentration of 5 mg/mL and 20 µL was added onto each sterile disc (5 mm). The plates were incubated overnight at 30 °C and the zones of inhibition were recorded (cm).

4.4. Bioactivity Agar Plug Assay

The 25 Polar strains were cultured in ISP2, ISP3, 10-fold diluted TSA and A1M1 media in 6-well plates (38 mm diameter/3 mL of media) until a uniform lawn was formed (25 °C, 7–14 days). Cultures in TSB (BD™) and LB [peptone 10 g/L, yeast extract 5g/L, NaCl 5 g/L] (5 mL, 30 °C, 1200 rpm, 12 h) were prepared for *Escherichia coli*, *Staphylococcus aureus*, *Klebsiella pneumoniae*, *Acinetobacter baumannii*, *Pseudomonas aeruginosa* and *Enterococcus faecalis*, respectively. NA (5 mL, Thermo Fisher Scientific) was inoculated with 0.1 mg/mL of the pathogen and poured onto NA (10 mL). Plugs (8 mm) from each bacterial lawn (grown for 14 days) were placed on the seeded pathogen plates and incubated overnight at 30 °C and the zones of inhibition were measured (cm).

4.5. Mass Spectral Data Acquisition

LC–MS/MS was performed using a Thermo Scientific Accela LC system coupled to a Thermo Finnigan LTQ Orbitrap mass spectrometer with an ESI source. Bacterial metabolite extracts and control media extracts (no bacteria) were prepared at 1 mg/mL in ACN and were injected onto an ACE 5 (Hichrom) C18 column (5 µm, 75 × 3.0 mm) using the following gradient: 1–5 min (5% ACN in H₂O), 5–25 min (5–100% ACN), 25–30 min (100% ACN). Mass data were collected in positive ion mode using ESI and mass range 150–1500 *m/z* (15,000 resolution). Data-dependent MS₂ scans were obtained using collision-induced dissociation (CID) with an energy of 35 eV and activation time of 30,000 ms for the first, second, and third most intense peaks.

4.6. Mass Spectral Data Processing

Mass spectral data were processed using MZmine v2.38 freeware (<http://mzmine.sourceforge.net/> (accessed on 9 November 2020)) for peak detection, deconvolution, deisotoping, filtering, alignment and gap filling to make multiple data files comparable. Throughout the data processing, the *m/z* tolerance used was 0.01, peaks were detected above 3.00E3 and the minimum time span and tR tolerance was 0.1 min. Mass detection was performed using a centroid mass detector with a noise level set at 2.00 × 10³.

4.7. Molecular Networking

The MS/MS data were converted from raw to mzXML file format using Proteowizard MSConvert [83] and the data were uploaded to the GNPS server [23]. A molecular network was created with the feature-based molecular networking workflow on the GNPS website (<http://gnps.ucsd.edu> (accessed on 9 November 2020)). The data were filtered by removing

all MS/MS fragment ions within ± 17 Da of the precursor m/z . MS/MS spectra were window filtered by choosing only the top 6 fragment ions in the ± 150 Da window throughout the spectrum. The precursor ion mass tolerance was set to 0.2 Da and a MS/MS fragment ion tolerance of 0.2 Da. A network was then created where edges were filtered to have a cosine score above 0.6 and at least 1 matched peak. Further, edges between two nodes were kept in the network if and only if each of the nodes appeared in each other's respective top 10 most similar nodes. Finally, the maximum size of a molecular family was set to 100, and the lowest scoring edges were removed from molecular families until the molecular family size was below this threshold. The spectra in the network were then searched against GNPS' spectral libraries. The library spectra were filtered in the same manner as the input data. All matches kept between network spectra and library spectra were required to have a score above 0.6 and at least 1 matched peak (<https://gnps.ucsd.edu/ProteoSAFe/status.jsp?task=124de327f32f474291a5037f41ac991d> (accessed on 9 November 2020)). For molecular network visualisation, Cytoscape version 3.6.1 was utilised [84] where each node corresponds to a consensus spectrum and each edge represents a modified cosine similarity score between nodes. The data used for the molecular networking analysis were deposited in the MassIVE Public GNPS database under access number MSV000086584.

4.8. MolNetEnhancer Workflow Description for Chemical Class Annotation of Molecular Networks

To enhance chemical structural information within the molecular network, information from in silico structure annotations from GNPS Library Search and Network Annotation Propagation (NAP) were incorporated into the network using the GNPS MolNetEnhancer workflow (<https://ccms-ucsd.github.io/GNPSDocumentation/molnetenhancer/> (accessed on 9 November 2020)) on the GNPS website [31]. Chemical class annotations were performed using the ClassyFire chemical ontology [85]. (<https://gnps.ucsd.edu/ProteoSAFe/status.jsp?task=adbadc0707e7449dbe4de1562ecd7bd3> (accessed on 9 November 2020)).

4.9. Genomic DNA Extraction

All 25 Polar strains were cultured in ISP2 medium (5 mL, 30 °C, 200 rpm for 3 days). High quality genomic DNA was isolated using an in-house protocol based on chemical cell lysis followed by phenol/chloroform extraction [86]. The *Pseudonocardia* sp. strains underwent cell lysis by vigorous vortexing (10 min) of the bacterial cultures with zirconium oxide beads (~0.5 g) (Sigma-Aldrich Ltd., Dorset, UK). The purity and concentration of the obtained genomic DNA was determined using a Nanodrop 2000 spectrophotometer (Thermo Fisher Scientific) followed by measurements on Qubit 2.0 Fluorometer (Invitrogen, Thermo Fisher Scientific, Waltham, MA, USA).

4.10. Genome Sequencing and Alignment

Whole-genome sequencing was carried out by Microbes NG (<https://microbesng.com/> (accessed on 9 November 2020)) as follows: Genomic DNA libraries were prepared using Nextera XT Library Prep Kit (Illumina, San Diego, CA, USA) following the manufacturer's protocol with the following modifications: two nanograms of DNA instead of one were used as input, and PCR elongation time was increased to 1 min from 30 s. DNA quantification and library preparation were carried out on a Hamilton Microlab STAR automated liquid handling system. Pooled libraries were quantified using the Kapa Biosystems Library Quantification Kit for Illumina on a Roche light cycler 96 qPCR machine. Libraries were sequenced on the Illumina HiSeq using a 250 bp paired-end protocol. Reads were adapter trimmed using Trimmomatic 0.30 with a sliding window quality cut off of Q15 [87]. The closest available reference genome was identified using Kraken [88] the reads were mapped with BWA mem for assessing the quality of the data. De novo assembly of the reads was carried out utilising SPAdes [89]. MeDuSa [90] was utilised for genome scaffolding, using reference strains with >95% similarity based on 16S rRNA sequencing data. The

Pseudonocardia isolates were not analysed by MeDuSa as no reference strains were identified. The whole genome sequences for the polar strains have been deposited to GenBank with the following accession numbers: SAMN14679891-SAMN14679907 (Table S2).

4.11. Biosynthetic Gene Cluster Mining and Comparison

The identification of BGCs was carried out using antiSMASH 5 beta [91]. The variety and number of BGCs each Polar strain was visualised using the Circos diagram [92]. The detected BGCs were grouped into Gene Cluster Families (GCF) using BiG-SCAPE 1.0 beta (Navarro-Munoz et al. 2019), with the underlying assumption that similar BGCs, i.e., BGCs that belong to the same GCF, produce similar metabolites. BiG-SCAPE was run using Longest Common Subcluster alignment mode, and cluster analysis carried out at the default cutoff of 0.3.

4.12. Computational Pattern Matching

Computational prioritisation of links between BGCs and candidate products made use of two complementary approaches. Firstly, the standardised strain correlation score described in [42] was used to compute a score between each spectrum and each GCF. The original strain correlation score introduced in [41] is heavily influenced by the number of strains present in each spectrum or GCF making the ranking of links between spectra and a particular GCF problematic. The standardised score overcomes this limitation, permitting a more balanced ranking of spectra for each GCF independent of their size. Significance values for each link were computed as described in [42]. Secondly, a novel approach named Rosetta (code available here: https://github.com/sdrogers/nplinker/tree/master/prototype/rosetta_data_prep (accessed on 9 November 2020)) based upon a set of collated matches between the GNPS [23] library spectra and the MiBIG database of characterised BGCs allows for putative links between individual spectra and BGCs to be highlighted. The set consists of 2960 links, 2069 unique spectra, 249 unique MiBIG IDs. To establish this set of collated links, the structural annotations available for both databases were used. A pair of objects from the two datasets were matched if the first blocks of the InChIKeys of the molecules in the GNPS library spectra and MiBIG validated gene cluster products matched. Matching was restricted to the first block to avoid distinguishing between molecules based on chemical properties that would not show up in the MS/MS spectra (e.g., stereochemistry). With this set of collated links, observed spectra and BGCs were putatively matched as follows: spectral similarity between measured MS2 spectra and the relevant subset of the GNPS spectra was computed using the modified cosine score (equivalent to “Analog search” in the GNPS framework). Results from antiSMASH were parsed to extract the known cluster blast results and Rosetta links between spectra and BGCs were generated where the spectra showed similarity to the GNPS spectrum and the MiBIG entry was found in the known cluster blast record for the BGC. All analysis was performed with the NPLinker framework [42] in which potential can be reported using either one of these two scoring methods, or both simultaneously, with user-defined thresholds.

Supplementary Materials: The following are available online at <https://www.mdpi.com/1660-3397/19/2/103/s1>, Figure S1: Molecular network of 3107 parent ions produced by 25 Polar actinomycete strains. Nodes are colour coded based on genus: *Agrococcus*, *Dietzia*, *Halomonas*, *Kocuria*, *Microbacterium*, *Micrococcus*, *Pseudonocardia* and *Rhodococcus*. Grey nodes represent media components, whereas orange nodes represent parent ions that are produced by more than one different medium. Figure S2: Pie chart showing the distribution of parent ions (%) between the 36 chemical class terms shown in the legend as annotated by MolNetEnhancer. The percentage of parent ions with no chemical class match (70.5%) is not shown in the pie chart. Each class has been colour coded to match the molecular network generated through MolNetEnhancer workflow analysis (Figure 5B). Table S1: Isolation and collection data of the 25 polar bacteria. Table S2: Genome quality of the Polar strains (*Pseudonocardia* strains were not analysed by MeDuSa as no reference strains were available). Table S3: Identified BGCs using antiSMASH 5 clusters after genome scaffolding using MeDuSa.

Table S4: Bioactive bacterial extracts organised by genus, strain name (KRD) and growth medium ISP3, A1M1, ISP2, and 10-fold dil. TSB. Antibiotic activity against the clinical pathogens *E. faecalis*, *S. aureus*, *K. pneumoniae*, *A. baumannii*, *P. aeruginosa* and *E. coli* is shown as zones of inhibition (cm) and colour coded by inhibition zone size. Table S5: Putatively identified metabolites using the Rosetta approach.

Author Contributions: Conceptualisation, K.R.D. and S.R.; methodology, S.S., G.H.E., S.R., and K.R.D.; formal analysis, S.S., G.H.E., S.R., and K.R.D.; investigation, S.S., G.H.E., A.H.H., S.R., and K.R.D.; writing—original draft preparation, S.S., G.H.E., S.R., and K.R.D.; writing—review and editing, S.S., G.H.E., A.R., J.J.J.v.d.H., A.H.H., S.R., and K.R.D.; supervision, K.R.D. and S.R.; project administration, K.R.D. and S.R. funding acquisition, K.R.D. and S.R. All authors have read and agreed to the published version of the manuscript.

Funding: This research was funded by Carnegie Trust Collaborative Research Grant (KRD, SR, SS). AR, KRD and SR were supported by the Biotechnology and Biological Sciences Research Council (BB/R022054/1). Additionally, genome sequencing was provided by MicrobesNG (<http://www.microbesng.uk> (accessed on 21 January 2021)) which was supported by the Biotechnology and Biological Sciences Research Council (BB/L024209/1).

Data Availability Statement: The code for Rosetta is available at https://github.com/sdrogers/nplinker/tree/master/prototype/rosetta_data_prep (accessed on 21 January 2021). The genomes have been deposited to GenBank with the following accession numbers: SAMN14679891–SAMN14679907 (Table S2). The GenBank accession numbers for the 16S rRNA gene sequences are the following: MT135519 (KRD153), MT135569 (KRD128), MT135795 (KR077), MT135986 (KRD070), MT136106 (KRD026), MT136242 (KRD012), MT136243 (KRD022), and MT136510 (KRD096) (Figure 1). The LC–MS data are available at the MassIVE dataset under access number MSV000086584.

Conflicts of Interest: The authors declare no conflict of interest.

References

- Davies, J.; Davies, D. Origins and Evolution of Antibiotic Resistance. *Microbiol. Mol. Biol. Rev.* **2010**, *74*, 417–433. [\[CrossRef\]](#)
- O' Neil, J. *Review on Antibiotic Resisitance. Antimicrobial Resistance: Tackling a Crisis for the Health and Wealth of Nations*; The Wellcome Trust and the UK Department of Health: London, UK, 2014.
- O' Neill, J. *Tackling Drug-Resistant Infections Globally: Final Report and Recommendations*; The Wellcome Trust and the UK Department of Health: London, UK, 2016.
- Jackson, S.A.; Crossman, L.; Almeida, E.L.; Margassery, L.M.; Kennedy, J.; Dobson, A.D.W. Diverse and Abundant Secondary Metabolism Biosynthetic Gene Clusters in the Genomes of Marine Sponge Derived *Streptomyces* spp. *Isolates. Mar. Drugs* **2018**, *16*, 67. [\[CrossRef\]](#)
- Baltz, R.H. Renaissance in Antibacterial Discovery from Actinomycetes. *Curr. Opin. Pharmacol.* **2008**, *8*, 557–563. [\[CrossRef\]](#) [\[PubMed\]](#)
- Lewin, G.R.; Carlos, C.; Chevrette, M.G.; Horn, H.A.; McDonald, B.R.; Stankey, R.J.; Fox, B.G.; Currie, C.R. Evolution and Ecology of Actinobacteria and Their Bioenergy Applications. *Annu. Rev. Microbiol.* **2016**, *70*, 235–254. [\[CrossRef\]](#) [\[PubMed\]](#)
- Baltz, R.H. Gifted Microbes for Genome Mining and Natural Product Discovery. *J. Ind. Microbiol. Biotechnol.* **2017**, *44*, 573–588. [\[CrossRef\]](#) [\[PubMed\]](#)
- Schorn, M.A.; Alanjary, M.M.; Aguinaldo, K.; Korobeynikov, A.; Podell, S.; Patin, N.; Lincecum, T.; Jensen, P.R.; Ziemert, N.; Moore, B.S. Sequencing Rare Marine Actinomycete Genomes Reveals High Density of Unique Natural Product Biosynthetic Gene Clusters. *Microbiology* **2016**, *162*, 2075–2086. [\[CrossRef\]](#) [\[PubMed\]](#)
- Letzel, A.-C.; Natalie, M.-A.; Amos, G.C.; Millán-Aguiñaga, N.; Ginigini, J.; Abdelmohsen, U.R.; Gaudêncio, S.P.; Ziemert, N.; Moore, B.S.; Jensen, P.R. Genomic Insights into Specialized Metabolism in the Marine Actinomycete *salinispora*. *Environ. Microbiol.* **2017**, *19*, 3660–3673. [\[CrossRef\]](#) [\[PubMed\]](#)
- Li, A.-Z.; Han, X.-B.; Zhang, M.-X.; Zhou, Y.; Chen, M.; Yao, Q.; Zhu, H.-H. Culture-Dependent and -Independent Analyses Reveal the Diversity, Structure, and Assembly Mechanism of Benthic Bacterial Community in the Ross Sea, Antarctica. *Front. Microbiol.* **2019**, *10*, 2523. [\[CrossRef\]](#)
- Millán-Aguiñaga, N.; Soldatou, S.; Brozio, S.; Munnoch, J.T.; Howe, J.A.; Hoskisson, P.A.; Duncan, K.R. Awakening Ancient Polar Actinobacteria: Diversity, Evolution and Specialized Metabolite Potential. *Microbiology* **2019**, *165*, 1169–1180. [\[CrossRef\]](#) [\[PubMed\]](#)
- Purves, K.; Macintyre, L.; Brennan, D.; Hreggviðsson, G.; Kuttner, E.; Ásgeirsdóttir, M.E.; Young, L.C.; Green, D.H.; Edrada-Ebel, R.; Duncan, K.R. Using Molecular Networking for Microbial Secondary Metabolite Bioprospecting. *Metabolites* **2016**, *6*, 2. [\[CrossRef\]](#)
- Tian, Y.; Taglialatela-Scafati, O.; Zhao, F. Secondary Metabolites from Polar Organisms. *Mar. Drugs* **2017**, *15*, 28. [\[CrossRef\]](#)

14. Gao, X.; Lu, Y.; Xing, Y.; Ma, Y.; Lu, J.; Bao, W.; Wang, Y.; Xi, T. A Novel Anticancer and Antifungus Phenazine Derivative from a Marine Actinomycete BM-17. *Microbiol. Res.* **2012**, *167*, 616–622. [[CrossRef](#)] [[PubMed](#)]
15. Zhang, H.; Saurav, K.; Yu, Z.; Mándi, A.; Kurtán, T.; Li, J.; Tian, X.; Zhang, Q.; Zhang, W.; Zhang, C. α -Pyrone with Diverse Hydroxy Substitutions from Three Marine-Derived *Nocardioopsis* Strains. *J. Nat. Prod.* **2016**, *79*, 1610–1618. [[CrossRef](#)] [[PubMed](#)]
16. Shin, H.J.; Mondol, M.M.; Yu, T.K.; Lee, H.-S.; Lee, Y.-J.; Jung, H.J.; Kim, J.H.; Kwon, H.J. An Angiogenesis Inhibitor Isolated from a Marine-Derived Actinomycete, *Nocardioopsis* sp. 03N67. *Phytochem. Lett.* **2010**, *3*, 194–197. [[CrossRef](#)]
17. Hoskisson, P.A.; Seipke, R.F. Cryptic or Silent? The Known Unknowns, Unknown Knowns, and Unknown Unknowns of Secondary Metabolism. *mBio* **2020**, *11*, 02642–20. [[CrossRef](#)]
18. Romano, S.; Jackson, S.A.; Patry, S.; Dobson, A.D.W. Extending the “One Strain Many Compounds” (Osmac) Principle to Marine Microorganisms. *Mar. Drugs* **2018**, *16*, 244. [[CrossRef](#)]
19. Rateb, M.E.; Houssen, W.E.; Harrison, W.T.A.; Deng, H.; Okoro, C.K.; Asenjo, J.A.; Andrews, B.A.; Bull, A.T.; Goodfellow, M.; Ebel, R.; et al. Diverse Metabolic Profiles of a *Streptomyces* Strain Isolated from a Hyper-Arid Environment. *J. Nat. Prod.* **2011**, *74*, 1965–1971. [[CrossRef](#)] [[PubMed](#)]
20. Che, Q.; Li, J.; Li, D.; Gu, Q.; Zhu, T. Structure and Absolute Configuration of Drimentine I, an Alkaloid from *Streptomyces* sp. CHQ-64. *J. Antibiot.* **2016**, *69*, 467–469. [[CrossRef](#)]
21. Che, Q.; Zhu, T.; Qi, X.; Mándi, A.; Kurtán, T.; Mo, X.; Li, J.; Gu, Q.; Li, D. Hybrid Isoprenoids from a Reeds Rhizosphere Soil Derived Actinomycete *Streptomyces* sp. CHQ-64. *Org. Lett.* **2012**, *14*, 3438–3441. [[CrossRef](#)]
22. Bode, H.B.; Bethe, B.; Höfs, R.; Zeck, A. Big Effects from Small Changes: Possible Ways to Explore Nature’s Chemical Diversity. *ChemBioChem* **2002**, *3*, 619–627. [[CrossRef](#)]
23. Wang, M.; Carver, J.J.; Phelan, V.V.; Sanchez, L.M.; Garg, N.; Peng, Y.; Nguyen, D.D.; Watrous, J.; Kapon, C.A.; Luzzatto-Knaan, T.; et al. Sharing and Community Curation of Mass Spectrometry Data with Global Natural Products Social Molecular Networking. *Nat. Biotechnol.* **2016**, *34*, 828–837. [[CrossRef](#)]
24. Quinn, R.A.; Nothias, L.F.; Vining, O.; Meehan, M.; Esquenazi, E.; Dorrestein, P.C. Molecular Networking As a Drug Discovery, Drug Metabolism, and Precision Medicine Strategy. *Trends Pharmacol. Sci.* **2017**, *38*, 143–154. [[CrossRef](#)] [[PubMed](#)]
25. Yang, J.Y.; Sanchez, L.M.; Rath, C.M.; Liu, X.; Boudreau, P.D.; Bruns, N.; Glukhov, E.; Wodtke, A.; De Felicio, R.; Fenner, A.; et al. Molecular Networking as a Dereplication Strategy. *J. Nat. Prod.* **2013**, *76*, 1686–1699. [[CrossRef](#)]
26. Audoin, C.; Zampalégré, A.; Blanchet, N.; Giuliani, A.; Roulland, E.; Laprévotte, O.; Genta-Jouve, G. MS/MS-Guided Isolation of Clarinoside, a New Anti-Inflammatory Pentalogin Derivative. *Molecules* **2018**, *23*, 1237. [[CrossRef](#)] [[PubMed](#)]
27. Duncan, K.R.; Crüsemann, M.; Lechner, A.; Sarkar, A.; Li, J.; Ziemert, N.; Wang, M.; Bandeira, N.; Moore, B.S.; Dorrestein, P.C.; et al. Molecular Networking and Pattern-Based Genome Mining Improves Discovery of Biosynthetic Gene Clusters and their Products from *Salinispora* Species. *Chem. Biol.* **2015**, *22*, 460–471. [[CrossRef](#)] [[PubMed](#)]
28. Nothias, L.-F.; Nothias-Esposito, M.; Da Silva, R.; Wang, M.; Protsyuk, I.; Zhang, Z.; Sarvepalli, A.; Leyssen, P.; Touboul, D.; Costa, J.; et al. Bioactivity-Based Molecular Networking for the Discovery of Drug Leads in Natural Product Bioassay-Guided Fractionation. *J. Nat. Prod.* **2018**, *81*, 758–767. [[CrossRef](#)]
29. Hooft, V.D.J.J.; Wandy, J.; Barrett, M.P.; Burgess, K.E.V.; Rogers, S. Topic Modeling for Untargeted Substructure Exploration in Metabolomics. *Proc. Natl. Acad. Sci. USA* **2016**, *113*, 13738–13743. [[CrossRef](#)]
30. Marchisio, M.A. In Silico Implementation of Synthetic Gene Networks BT-Synthetic Gene Networks: Methods and Protocols. *Methods Mol. Biol.* **2012**, *813*, 3–21.
31. Ernst, M.; Bin Kang, K.; Caraballo-Rodríguez, A.M.; Nothias, L.-F.; Wandy, J.; Chen, C.; Wang, M.; Rogers, S.; Medema, M.H.; Dorrestein, P.C.; et al. MolNetEnhancer: Enhanced Molecular Networks by Integrating Metabolome Mining and Annotation Tools. *Metabolites* **2019**, *9*, 144. [[CrossRef](#)]
32. Bentley, S.D.; Chater, K.F.; Cerdeño-Tárraga, A.-M.; Challis, G.L.; Thomson, N.R.; James, K.D.; Harris, D.E.; Quail, M.; Kieser, H.M.; Harper, D.P.; et al. Complete Genome Sequence of the Model Actinomycete *Streptomyces Coelicolor* A3(2). *Nat. Cell Biol.* **2002**, *417*, 141–147. [[CrossRef](#)]
33. Machado, H.; Tuttle, R.N.; Jensen, P.R. Omics-Based Natural Product Discovery and the Lexicon of Genome Mining. *Curr. Opin. Microbiol.* **2017**, *39*, 136–142. [[CrossRef](#)] [[PubMed](#)]
34. Ziemert, N.; Alanjary, M.; Weber, T. The Evolution of Genome Mining in Microbes—A Review. *Nat. Prod. Rep.* **2016**, *33*, 988–1005. [[CrossRef](#)] [[PubMed](#)]
35. Medema, M.H.; Fischbach, M.A. Computational Approaches to Natural Product Discovery. *Nat. Chem. Biol.* **2015**, *11*, 639–648. [[CrossRef](#)] [[PubMed](#)]
36. Blin, K.; Medema, M.H.; Kottmann, R.; Lee, S.Y.; Weber, T. The AntiSMASH Database, a Comprehensive Database of Microbial Secondary Metabolite Biosynthetic Gene Clusters. *Nucleic Acids Res.* **2017**, *45*, D555–D559. [[CrossRef](#)] [[PubMed](#)]
37. Alanjary, M.; Kronmiller, B.; Adamek, M.; Blin, K.; Weber, T.; Huson, D.H.; Philmus, B.; Ziemert, N. The Antibiotic Resistant Target Seeker (ARTS), An Exploration Engine for Antibiotic Cluster Prioritization and Novel Drug Target Discovery. *Nucleic Acids Res.* **2017**, *45*, W42–W48. [[CrossRef](#)]
38. Navarro-Muñoz, J.C.; Selem-Mojica, N.; Mullowney, M.W.; Kautsar, S.A.; Tryon, J.H.; Parkinson, E.I.; Santos, E.L.C.D.L.; Yeong, M.; Cruz-Morales, P.; Abubucker, S.; et al. A Computational Framework to Explore Large-Scale Biosynthetic Diversity. *Nat. Chem. Biol.* **2020**, *16*, 60–68. [[CrossRef](#)]

39. Soldatou, S.; Eldjarn, G.H.; Huerta-Urbe, A.; Rogers, S.; Duncan, K.R. Linking Biosynthetic and Chemical Space to Accelerate Microbial Secondary Metabolite Discovery. *FEMS Microbiol. Lett.* **2019**, *366*, 142. [[CrossRef](#)]
40. Goering, A.W.; McClure, R.A.; Doroghazi, J.R.; Albright, J.C.; Haverland, N.A.; Zhang, Y.; Ju, K.S.; Thomson, R.J.; Metcalf, W.W.; Kelleher, N.L. Metabologenomics: Correlation of Microbial Gene Clusters with Metabolites Drives Discovery of a Non-Ribosomal Peptide with an Unusual Amino Acid Monomer. *ACS Cent. Sci.* **2016**, *2*, 99–108. [[CrossRef](#)]
41. Doroghazi, J.R.; Albright, J.C.; Goering, A.W.; Ju, K.S.; Haines, R.R.; Tchalukov, K.A.; Labeda, D.P.; Kelleher, N.L.; Metcalf, W.W. A Roadmap for Natural Product Discovery Based on Large-Scale Genomics and Metabolomics. *Nat. Chem. Biol.* **2014**, *10*, 963–968. [[CrossRef](#)]
42. Eldjárn, G.H.; Ramsay, A.; van der Hooft, J.J.J.; Duncan, K.R.; Soldatou, S.; Rousu, J.; Daly, R.; Wandy, J.; Rogers, S. Ranking Microbial Metabolomic and Genomic Links in the NPLinker Framework Using Complementary Scoring Functions. *bioRxiv* **2020**. [[CrossRef](#)]
43. Fenical, W.; Jensen, P.R. Developing a New Resource for Drug Discovery: Marine Actinomycete Bacteria. *Nat. Chem. Biol.* **2006**, *2*, 666–673. [[CrossRef](#)] [[PubMed](#)]
44. Pickens, L.B.; Kim, W.; Wang, P.; Zhou, H.; Watanabe, K.; Gomi, S.; Tang, Y. Biochemical Analysis of the Biosynthetic Pathway of an Anticancer Tetracycline SF2575. *J. Am. Chem. Soc.* **2009**, *131*, 17677–17689. [[CrossRef](#)] [[PubMed](#)]
45. Hatsu, M.; Sasaki, T.; Watabe, H.-O.; Miyadoh, S.; Nagasawa, M.; Shomura, T.; Sezaki, M.; Inouye, S.; Kondo, S. A New Tetracycline Antibiotic with Antitumor Activity. I. Taxonomy and Fermentation of the Producing Strain, Isolation and Characterization of SF2575. *J. Antibiot.* **1992**, *45*, 320–324. [[CrossRef](#)] [[PubMed](#)]
46. Fernández-Martínez, L.T.; Borsetto, C.; Gomez-Escribano, J.P.; Bibb, M.J.; Al-Bassam, M.M.; Chandra, G.; Bibb, M. New Insights into Chloramphenicol Biosynthesis in *Streptomyces venezuelae* ATCC 10712. *Antimicrob. Agents Chemother.* **2014**, *58*, 7441–7450. [[CrossRef](#)]
47. Kleijn, L.H.J.; Martin, N.I. The Cyclic Lipopeptide Antibiotics. In *Antibacterials. Topics in Medicinal Chemistry*; Fisher, J.F., Mobashery, S., Miller, M.J., Eds.; Springer International Publishing: Cham, Switzerland, 2018; pp. 27–53. ISBN 978-3-319-70839-3.
48. Rice, L.B. Federal Funding for the Study of Antimicrobial Resistance in Nosocomial Pathogens: No ESKAPE. *J. Infect. Dis.* **2008**, *197*, 1079–1081. [[CrossRef](#)] [[PubMed](#)]
49. Yan, Y.; Zhang, L.; Ito, T.; Qu, X.; Asakawa, Y.; Awakawa, T.; Abe, I.; Liu, W. Biosynthetic Pathway for High Structural Diversity of a Common Dilactone Core in Antimycin Production. *Org. Lett.* **2012**, *14*, 4142–4145. [[CrossRef](#)]
50. Westley, J.W.; Liu, C.-M.; Evans, R.H.; Blount, J.F. Conglobatin, a Novel Macrolide Dilactone from *Streptomyces conglobatus* ATCC 31005. *J. Antibiot.* **1979**, *32*, 874–877. [[CrossRef](#)]
51. Zhou, Y.; Murphy, A.C.; Samborsky, M.; Prediger, P.; Dias, L.C.; Leadlay, P.F. Iterative Mechanism of Macrolide Formation in the Anticancer Compound Conglobatin. *Chem. Biol.* **2015**, *22*, 745–754. [[CrossRef](#)] [[PubMed](#)]
52. Rebstock, M.C.; Crooks, H.M.; Controulis, J.; Bartz, Q.R. Chloramphenicol (Chloromycetin). IIV.1a Chemical Studies. *J. Am. Chem. Soc.* **1949**, *71*, 2458–2462. [[CrossRef](#)]
53. Van Der Hooft, J.J.J.; Mohimani, H.; Bauermeister, A.; Dorrestein, P.C.; Duncan, K.R.; Medema, M.H. Linking Genomics and Metabolomics to Chart Specialized Metabolic Diversity. *Chem. Soc. Rev.* **2020**, *49*, 3297–3314. [[CrossRef](#)]
54. Medema, M.H.; Blin, K.; Cimermancic, P.; De Jager, V.; Zakrzewski, P.; Fischbach, M.A.; Weber, T.; Takano, E.; Breitling, R. antiSMASH: Rapid Identification, Annotation and Analysis of Secondary Metabolite Biosynthesis Gene Clusters in Bacterial and Fungal Genomes. *Nucleic Acids Res.* **2011**, *39*, W339–W346. [[CrossRef](#)]
55. Klassen, J.L.; Currie, C.R. Gene Fragmentation in Bacterial Draft Genomes: Extent, Consequences and Mitigation. *BMC Genom.* **2012**, *13*, 14. [[CrossRef](#)] [[PubMed](#)]
56. Goldstein, S.; Beka, L.; Graf, J.; Klassen, J.L. Evaluation of Strategies for the Assembly of Diverse Bacterial Genomes Using Minion Long-Read Sequencing. *BMC Genom.* **2019**, *20*, 23. [[CrossRef](#)] [[PubMed](#)]
57. Baltz, R.H. Molecular Beacons to Identify Gifted Microbes for Genome Mining. *J. Antibiot.* **2017**, *70*, 639–646. [[CrossRef](#)] [[PubMed](#)]
58. Smits, T.H.M. The Importance of Genome Sequence Quality to Microbial Comparative Genomics. *BMC Genom.* **2019**, *20*, 1–4. [[CrossRef](#)]
59. Yamada, Y.; Kuzuyama, T.; Komatsu, M.; Shin-ya, K.; Omura, S.; Cane, D.E.; Ikeda, H. Terpene Synthases Are Widely Distributed in Bacteria. *Proc. Natl. Acad. Sci. USA* **2015**, *112*, 857–862. [[CrossRef](#)]
60. Blodgett, J.A.V.; Oh, D.-C.; Cao, S.; Currie, C.R.; Kolter, R.; Clardy, J. Common Biosynthetic Origins for Polycyclic Tetramate Macrolactams from Phylogenetically Diverse Bacteria. *Proc. Natl. Acad. Sci. USA* **2010**, *107*, 11692–11697. [[CrossRef](#)]
61. Li, S.; Li, Y.; Lu, C.; Zhang, J.; Zhu, J.; Wang, H.; Shen, Y. Activating a Cryptic Ansamycin Biosynthetic Gene Cluster To Produce Three New Naphthalenic Octaketide Ansamycins with n-Pentyl and n-Butyl Side Chains. *Org. Lett.* **2015**, *17*, 3706–3709. [[CrossRef](#)]
62. Eltamany, E.E.; Abdelmohsen, U.R.; Ibrahim, A.K.; Hassanean, H.A.; Hentschel, U.; Ahmed, S.A. New Antibacterial Xan-Thone from the Marine Sponge-Derived *Micrococcus* sp. EG45. *Bioorg. Med. Chem. Lett.* **2014**, *24*, 4939–4942. [[CrossRef](#)]
63. Homann, V.V.; Sandy, M.; Tincu, J.A.; Templeton, A.S.; Tebo, B.M.; Butler, A. Loihichelins A–F, a Suite of Amphiphilic Siderophores Produced by the Marine Bacterium *Halomonas* LOB-5. *J. Nat. Prod.* **2009**, *72*, 884–888. [[CrossRef](#)]
64. Bitzer, J.; Grosse, T.; Wang, L.; Lang, S.; Beil, W.; Zeeck, A. New Aminophenoxazinones from a Marine *Halomonas* sp.: Fermentation, Structure Elucidation, and Biological Activity. *J. Antibiot.* **2006**, *59*, 86–92. [[CrossRef](#)] [[PubMed](#)]

65. Czech, L.; Hermann, L.; Stöveken, N.; Richter, A.A.; Höppner, A.; Smits, S.H.J.; Heider, J.; Bremer, E. Role of the Extremolytes Ectoine and Hydroxyectoine as Stress Protectants and Nutrients: Genetics, Phylogenomics, Biochemistry, and Structural Analysis. *Genes* **2018**, *9*, 177. [[CrossRef](#)] [[PubMed](#)]
66. Schweiggert, R.; Carle, R. Carotenoid Deposition in Plant And Animal Foods and Its Impact on Bioavailability. *Crit. Rev. Food Sci. Nutr.* **2015**, *57*. [[CrossRef](#)] [[PubMed](#)]
67. Iftime, D.; Kulik, A.; Härtner, T.; Rohrer, S.; Niedermeyer, T.H.J.; Stegmann, E.; Weber, T.; Wohlleben, W. Identification and Activation of Novel Biosynthetic Gene Clusters by Genome Mining in the Kirromycin Producer *Streptomyces collinus* Tü 365. *J. Ind. Microbiol. Biotechnol.* **2016**, *43*, 277–291. [[CrossRef](#)]
68. Myronovskiy, M.; Tokovenko, B.; Brötz, E.; Rückert, C.; Kalinowski, J.; Luzhetskyy, A. Genome Rearrangements of *Streptomyces Albus* J1074 Lead to the Carotenoid Gene Cluster Activation. *Appl. Microbiol. Biotechnol.* **2014**, *98*, 795–806. [[CrossRef](#)]
69. Debono, M.; Barnhart, M.; Carrell, C.B.; Hoffmann, J.A.; Occolowitz, J.L.; Abbott, B.J.; Fukuda, D.S.; Hamill, R.L.; Biemann, K.; Herlihy, W.C. A21978C, A Complex of New Acidic Peptide Antibiotics. Isolation, Chemistry, and Mass Spectral Structure Elucidation. *J. Antibiot.* **1987**, *40*, 761–777. [[CrossRef](#)]
70. Kosmidis, C.; Levine, D.P. Daptomycin: Pharmacology and Clinical Use. *Expert Opin. Pharmacother.* **2010**, *11*, 615–625. [[CrossRef](#)]
71. Balouiri, M.; Sadiki, M.; Ibsouda, S.K. Methods for in Vitro Evaluating Antimicrobial Activity: A Review. *J. Pharm. Anal.* **2016**, *6*, 71–79. [[CrossRef](#)]
72. Paczosa, M.K.; Meccas, J. *Klebsiella pneumoniae*: Going on the Offense with a Strong Defense. *Microbiol. Mol. Biol. Rev.* **2016**, *80*, 629–661. [[CrossRef](#)]
73. Chapartegui-González, I.; Lázaro-Díez, M.; Bravo, Z.; Navas, J.; Icardo, J.M.; Ramos-Vivas, J. *Acinetobacter baumannii* Maintains Its Virulence after Long-Time Starvation. *PLoS ONE* **2018**, *13*, e0201961. [[CrossRef](#)]
74. Liaw, C.-C.; Chen, P.-C.; Shih, C.-J.; Tseng, S.-P.; Lai, Y.-M.; Hsu, C.-H.; Dorrestein, P.C.; Yang, Y. Vitroprocines, New Antibiotics against *Acinetobacter baumannii*, Discovered from Marine *Vibrio* SP. QWI-06 Using Mass-Spectrometry-Based Metabolomics Approach. *Sci. Rep.* **2015**, *5*, 12856. [[CrossRef](#)]
75. Vila-Farres, X.; Chu, J.; Ternei, M.A.; Lemetre, C.; Park, S.; Perlin, D.S.; Brady, S.F. An Optimized Synthetic-Bioinformatic Natural Product Antibiotic Sterilizes Multidrug-Resistant *Acinetobacter baumannii*-Infected Wounds. *mSphere* **2018**, *3*, e00528-17. [[CrossRef](#)]
76. Wu, W.-S.; Cheng, W.-C.; Cheng, T.-J.R.; Wong, C.-H. Affinity-Based Screen for Inhibitors of Bacterial Transglycosylase. *J. Am. Chem. Soc.* **2018**, *140*, 2752–2755. [[CrossRef](#)]
77. Zdouc, M.M.; Iorio, M.; Maffioli, S.I.; Crüsemann, M.; Donadio, S.; Sosio, M. *Planomonospora*: A Metabolomics Perspective on an Underexplored Actinobacteria Genus. *J. Nat. Prod.* **2021**. [[CrossRef](#)] [[PubMed](#)]
78. Van Santen, J.A.; Kautsar, S.A.; Medema, M.H.; Lington, R.G. Microbial Natural Product Databases: Moving Forward in the Multiomics Era. *Nat. Prod. Rep.* **2021**, *38*, 264–278. [[CrossRef](#)] [[PubMed](#)]
79. Kurita, K.L.; Glassey, E.; Lington, R.G. Integration of High-Content Screening and Untargeted Metabolomics for Comprehensive Functional Annotation of Natural Product Libraries. *Proc. Natl. Acad. Sci. USA* **2015**, *112*, 11999–12004. [[CrossRef](#)]
80. Kimura, M. A Simple Method for Estimating Evolutionary Rates of Base Substitutions through Comparative Studies of Nucleotide Sequences. *J. Mol. Evol.* **1980**, *16*, 111–120. [[CrossRef](#)] [[PubMed](#)]
81. Kumar, S.; Stecher, G.; Tamura, K. MEGA7: Molecular Evolutionary Genetics Analysis Version 7.0 for Bigger Datasets. *Mol. Biol. Evol.* **2016**, *33*, 1870–1874. [[CrossRef](#)]
82. Shirling, E.B.; Gottlieb, D. Methods for Characterization of *Streptomyces* Species. *Int. J. Syst. Bacteriol.* **1966**, *16*, 313–340. [[CrossRef](#)]
83. Adusumilli, R.; Mallick, P. Data Conversion with Proteo Wizard msConvert. In *Proteomics*; Springer: Berlin/Heidelberg, Germany, 2017; pp. 339–368.
84. Cline, M.S.; Smoot, M.; Cerami, E.; Kuchinsky, A.; Landys, N.; Workman, C.; Christmas, R.; Avila-Campilo, I.; Creech, M.; Gross, B.; et al. Integration of Biological Networks and Gene Expression Data Using Cytoscape. *Nat. Protoc.* **2007**, *2*, 2366–2382. [[CrossRef](#)]
85. Djoumbou Feunang, Y.; Eisner, R.; Knox, C.; Chepelev, L.; Hastings, J.; Owen, G.; Fahy, E.; Steinbeck, C.; Subramanian, S.; Bolton, E.; et al. Classyfire: Automated Chemical Classification with a Comprehensive, Computable Taxonomy. *J. Cheminform.* **2016**, *8*, 61. [[CrossRef](#)]
86. Sambrook, J.; Maniatis, T.; Fritsch, E.F. *Molecular Cloning: A Laboratory Manual*, 2nd ed.; Cold Spring Harbor Laboratory Press: New York, NY, USA, 1989.
87. Bolger, A.M.; Lohse, M.; Usadel, B. Trimmomatic: A Flexible Trimmer for Illumina Sequence Data. *Bioinformatics* **2014**, *30*, 2114–2120. [[CrossRef](#)]
88. Wood, E.; Salzberg, D.E.; Kraken, S.L. Ultrafast Metagenomic Sequence Classification Using Exact Alignments. *Genome Biol.* **2014**, *15*, R46. [[CrossRef](#)] [[PubMed](#)]
89. Bankevich, A.; Nurk, S.; Antipov, D.; Gurevich, A.A.; Dvorkin, M.; Kulikov, A.S.; Lesin, V.M.; Nikolenko, S.I.; Pham, S.; Prjibelski, A.D.; et al. SPAdes: A New Genome Assembly Algorithm and Its Applications to Single-Cell Sequencing. *J. Comput. Biol.* **2012**, *19*, 455–477. [[CrossRef](#)] [[PubMed](#)]
90. Bosi, E.; Donati, B.; Galardini, M.; Brunetti, S.; Sagot, M.-F.; Lió, P.; Crescenzi, P.; Fani, R.; Fondi, M. MeDuSa: A Multi-Draft Based Scaffold. *Bioinformatics* **2015**, *31*, 2443–2451. [[CrossRef](#)]

-
91. Blin, K.; Shaw, S.; Steinke, K.; Villebro, R.; Ziemert, N.; Lee, S.Y.; Medema, M.H.; Weber, T. antiSMASH 5.0: Updates to the Secondary Metabolite Genome Mining Pipeline. *Nucleic Acids Res.* **2019**, *47*, W81–W87. [[CrossRef](#)] [[PubMed](#)]
 92. Krzywinski, M.; Schein, J.; Birol, I.; Connors, J.; Gascoyne, R.; Horsman, D.; Jones, S.J.; Marra, M.A. Circos: An Information Aesthetic for Comparative Genomics. *Genome Res.* **2009**, *19*, 1639–1645. [[CrossRef](#)] [[PubMed](#)]

Table S1: Isolation and collection data of the 25 polar bacteria.

Ref. No	Closest type stain	Polar region	Location	Year of collection	Length (cm)	Type	Depth (m)	Section (B, M, U)
KRD012	<i>Micrococcus</i> sp.	Antarctica	Antarctic PS61-139	N/R	N/R	N/R	N/R	N/A
KRD022	<i>Micrococcus</i> sp.	Antarctica	PS67-16A, Agullas Basin	2005	N/R	Box	4730	N/A
KRD026	<i>Micrococcus</i> sp.	Antarctica	PS67-16A, Agullas Basin	2005	N/R	Box	4730	N/A
KRD070	<i>Micrococcus</i> sp.	Arctic	M5M-75-62-B4, Voring Plateau	2002	N/R	Gravity	1358	N/A
KRD077	<i>Micrococcus</i> sp.	Arctic	M5M-75-62-B4, Voring Plateau	2002	N/R	Gravity	1358	N/A
KRD096	<i>Micrococcus</i> sp.	Arctic	M5M-127b-99b8, Kongsfjord Outer	2005	N/R	Piston	388	N/A
KRD128	<i>Micrococcus</i> sp.	Arctic	M5M-219-143A, Northern Svalbard Margin	2007	N/R	Piston	N/R	N/A
KRD140	<i>Kocuria</i> sp.	Antarctica	Antarctic PS66-88A, Weddell Abyssal P.	205	N/R	multi	4932	N/A
KRD153	<i>Micrococcus</i> sp.	Arctic	M5M-219-142B	N/R	N/R	N/R	N/R	N/R
KRD162	<i>Rhodococcus</i> sp.	Antarctica	PS61 138-8 (BC052-A)	2002	38	Box	4539	B
KRD168	<i>Pseudonocardia</i> sp.	Antarctica	PS61 138-8 (BC052-A)	2002	38	Box	4539	B
KRD169	<i>Pseudonocardia</i> sp.	Antarctica	PS61 138-8 (BC052-A)	2002	38	Box	4539	B
KRD171	<i>Halomonas</i> sp.	Arctic	JR75 (GC067)	2002	77	Gravity	1226	M
KRD172	<i>Microbacterium</i> sp.	Arctic	JR75 (GC067)	2002	77	Gravity	1226	M
KRD174	<i>Microbacterium</i> sp.	Arctic	JR75 (GC067)	2002	77	Gravity	1226	M
KRD175	<i>Rhodococcus</i> sp.	Arctic	JR75 (GC067)	2002	77	Gravity	1226	B
KRD176	<i>Pseudonocardia</i> sp.	Antarctica	PS61 134-5 (BC043)	2002	45.5	Box	4060	U
KRD182	<i>Pseudonocardia</i> sp.	Antarctica	PS61 134-5 (BC043)	2002	45.5	Box	4060	U
KRD184	<i>Pseudonocardia</i> sp.	Antarctica	PS61 134-5 (BC043)	2002	45.5	Box	4060	M
KRD185	<i>Pseudonocardia</i> sp.	Antarctica	PS61 134-5 (BC043)	2002	45.5	Box	4060	M
KRD186	<i>Agrococcus</i> sp.	Antarctica	PS61 134-5 (BC043)	2002	45.5	Box	4060	B
KRD188	<i>Pseudonocardia</i> sp.	Antarctica	PS61 134-5 (BC043)	2002	45.5	Box	4060	B
KRD291	<i>Pseudonocardia</i> sp.	Antarctica	PS61 134-5 (BC043)	2002	45.5	Box	4060	B
KRD197	<i>Rhodococcus</i> sp.	Antarctica	PS61 140-2 (BC055W)	2002	16	Box	2946	U
KRD202	<i>Dietzia</i> sp.	Arctic	JR219 PC141	2010	86.5	Piston	N/R	N/R

N/R: Not recorded, N/A: Not Applicable. Section (B, M, U): section of the core where the sample was taken; B: Bottom, M: Middle, U: Upper

[Type here]

Table S2: Genome quality of the Polar strains. (*Pseudonocardia* strains were not analysed by MeDuSa as no reference strains were available)

Strain	GenBank accession number	Most frequent family (%)	Most frequent species (%)	Number of reads	GC (%)	Number of contigs	Total length (bp)	N50
KRD 012	SAMN14679891	Micrococcaceae (86.32)	<i>Micrococcus luteus</i> (86.13)	587934	73,14	54	2428345	152950
KRD 022	SAMN14679892	Micrococcaceae (87.14)	<i>Micrococcus luteus</i> (86.94)	991624	72,5	634	2708943	48082
KRD 026	SAMN14679893	Micrococcaceae (84.08)	<i>Micrococcus luteus</i> (83.67)	777451	72,72	93	2630609	126029
KRD 070	SAMN14679894	Micrococcaceae (84.26)	<i>Micrococcus luteus</i> (84.04)	860196	72,96	61	2506630	120226
KRD 077	SAMN14679895	Micrococcaceae (86.50)	<i>Micrococcus luteus</i> (85.18)	897931	72,79	117	2553835	77566
KRD 096	SAMN14679896	Micrococcaceae (87.02)	<i>Micrococcus luteus</i> (86.67)	335398	72,99	91	2499004	167875
KRD 128	SAMN14679897	Micrococcaceae (85.88)	<i>Micrococcus luteus</i> (85.37)	112082 6	73,19	69	2447759	166662
KRD 140	SAMN14679898	Micrococcaceae (34.9)	<i>Kocuria rhizophila</i> (32.10)	253418	68,91	36	2743959	503418
KRD 153	SAMN14679899	Micrococcaceae (87.30)	<i>Micrococcus luteus</i> (87.09)	201536 7	72,87	82	2546919	127028
KRD 162	SAMN14679900	Nocardiaceae (10.26)	<i>Rhodococcus erythropolis</i> (3.16)	470260	64,22	110	5901029	339827
KRD 171	SAMN14679901	Halomonadaceae (2.03)	<i>Halomonas elongata</i> (1.20)	577377	54,66	57	5542288	425172
KRD 172	SAMN14679902	Microbacteriaceae (7.91)	<i>Microbacterium testaceum</i> (4.77)	439847	66,7	38	3362075	319652 4
KRD 174	SAMN14679903	Microbacteriaceae (8.27)	<i>Microbacterium testaceum</i> (4.93)	104910 2	66,53	452	4823384	106614
KRD 175	SAMN14679904	Nocardiaceae (9.63)	<i>Rhodococcus erythropolis</i> (2.55)	603595	64,67	82	5449128	432516
KRD 186	SAMN14679905	Microbacteriaceae (6.32)	<i>Clavibacter michiganensis</i> (3.34)	293168	70,97	29	3101783	304870 3
KRD 197	SAMN14679906	Nocardiaceae (7.72)	<i>Rhodococcus erythropolis</i> (1.59)	569376	64,12	296	6781538	736182
KRD 202	SAMN14679907	Nocardiaceae (5.01)	<i>Rhodococcus pyridinivorans</i> (0.87)	772984	70,01	101	5564907	341290

N50: the length for which the collection of all contigs of that length or longer covers at least half an assembly

[Type here]

Table S3: Identified BGCs using antiSMASH 5 clusters after genome scaffolding using MeDuSa

Strain	Genus	Total Clusters	NRPS	NRPS-like	Type 1 PKS	Type 2 PKS	Type 3 PKS	hglE-KS	Terpene	Betalactone	Siderophore	Butyrolactone	Arylpolyene	Ectoine	LAP	Lasso peptide	Bacteriocin	Hybrid	Hybrid types
KRD012	Micrococcus	5	0	1	0	0	0	0	1	1	1	0	0	1	0	0	0	0	-
KRD022	Micrococcus	5	0	1	0	0	0	0	1	1	1	0	0	1	0	0	0	0	-
KRD026	Micrococcus	6	0	1	0	0	0	0	1	1	1	0	0	1	0	0	0	1	Arylpolyene-NRPS
KRD070	Micrococcus	5	0	1	0	0	0	0	1	1	1	0	0	1	0	0	0	0	-
KRD077	Micrococcus	5	0	1	0	0	0	0	1	1	1	0	0	1	0	0	0	0	-
KRD096	Micrococcus	5	0	1	0	0	0	0	1	1	1	0	0	1	0	0	0	0	-
KRD128	Micrococcus	5	0	1	0	0	0	0	1	1	1	0	0	1	0	0	0	0	-
KRD140	Kocuria	5	0	1	0	0	1	0	1	1	1	0	0	0	0	0	0	0	-
KRD153	Micrococcus	5	0	1	0	0	0	0	1	1	1	0	0	1	0	0	0	0	-
KRD162	Rhodococcus	21	8	6	1	0	0	0	2	0	0	1	0	1	0	1	0	1	Lantipeptide/Ladderane
KRD171	Halomonas	4	1	0	1	0	0	0	0	1	0	0	0	1	0	0	0	0	-
KRD172	Microbacterium	5	0	2	0	0	0	0	1	0	0	0	0	1	0	0	0	1	t3PKS/ betalactone
KRD174	Microbacterium	5	0	2	0	0	1	0	1	1	0	0	0	0	0	0	0	0	-
KRD175	Rhodococcus	17	6	4	1	0	0	0	2	0	0	1	1	1	0	0	1	0	-
KRD186	Agrococcus	5	0	1	0	0	1	0	1	1	0	0	0	1	0	0	0	0	-
KRD197	Rhodococcus	22	10	2	1	1	0	1	2	0	0	0	0	1	1	0	0	3	Butyrolactone/NRPS, NRPS-like/Arylpolyene, PKS-like/t1PKS/Arylpolyene
KRD202	Dietzia	7	1	1	1	0	0	0	2	0	1	0	0	1	0	0	0	0	-

[Type here]

Table S4: Bioactive bacterial extracts organised by genus, strain name (KRD) and growth medium ISP3, A1M1, ISP2, and 10-fold dil. TSB. Antibiotic activity against the clinical pathogens *E. faecalis*, *S. aureus*, *K. pneumoniae*, *A. baumannii*, *P. aeruginosa* and *E. coli* is shown as zones of inhibition (cm) and colour coded by inhibition zone size.

Genus	Strain	Growth medium	<i>E. faecalis</i>	<i>S.aureus</i>	<i>K. pneumoniae</i>	<i>A. baumannii</i>	<i>P. aeruginosa</i>	<i>E.coli</i>
<i>Micrococcus</i> sp.	KRD026	ISP2	-	0,5	-	-	-	-
		M1	-	0,4	-	-	-	0,3
<i>Micrococcus</i> sp.	KRD070	ISP2	-	0,3	-	-	-	0,1
<i>Micrococcus</i> sp.	KRD077	ISP2	-	0,3	-	0,1	-	0,1
		ISP3	-	-	-	-	0,2	-
		M1	-	-	-	-	0,3	-
		TSB	-	-	-	-	0,2	-
<i>Micrococcus</i> sp.	KRD096	ISP2	-	-	-	-	0,1	
<i>Micrococcus</i> sp.	KRD153	ISP2	-	0,3	-	-	-	-
		M1	-	-	-	-	0,2	0,1
		TSB	-	-	-	-	0,1	-
<i>Pseudonocardia</i> sp.	KRD168	ISP3	-	0,7	-	-	-	
<i>Pseudonocardia</i> sp.	KRD182	ISP3	-	0,8	-	-	-	-
		TSB	-	0,7	-	-	-	-
<i>Pseudonocardia</i> sp.	KRD185	ISP3	0,6	-	-	-	-	-
		M1	-	2,1	0,9	1,5	2,1	0,9
<i>Pseudonocardia</i> sp.	KRD188	ISP3	-	0,3	-	-	-	0,2
<i>Rhodococcus</i> sp.	KRD175	M1	-	-	0,4	-	-	-
		TSB	-	-	0,5	-	-	-
<i>Kocuria</i> sp.	KRD140	ISP2	-	0,6	-	-	-	0,4
		ISP3	-	-	-	-	-	0,3
		M1	-	0,4	-	-	-	0,3

[Type here]

Table S5: Putatively identified metabolites using the Rosetta approach.

Compound	GNPS Spectrum ID	GNPS Library ID	m/z	Metabolomics Spectrum Resolver URL
Antimycin-like	225126	CCMSLIB0000569369	547.3815	https://www.google.com/url?q=https://metabolomics-usi.ucsd.edu/mirror?usi1%3Dmzspec:GNPS:TASK-124de327f32f474291a5037f41ac991d-spectra/specs_ms.mgf:scan:225126%26usi2%3Dmzspec:GNPS:GNPS-LIBRARY:accession:CCMSLIB00000569369%26width%3D10.0%26height%3D6.0%26mz_min%3D%26mz_max%3D%26max_intensity%3D150.0%26grid%3Dtrue%26annotate_peaks%3D%5B%5B547.3823%5D,%5B101.0603,219.0767,245.0553,401.2062,547.2642%5D%5D%26annotate_precision%3D4%26annotation_rotation%3D90%26cosine%3Dstandard%26fragment_mz_tolerance%3D0.2&sa=D&ust=1604063429163000&usg=AOvVaw2P1sMf6ulSDwba9JbJ0cB
Conglobatin-like	200494	CCMSLIB0004710288	521.3294	https://www.google.com/url?q=https://metabolomics-usi.ucsd.edu/mirror?usi1%3Dmzspec:GNPS:TASK-124de327f32f474291a5037f41ac991d-spectra/specs_ms.mgf:scan:200494%26usi2%3Dmzspec:GNPS:GNPS-LIBRARY:accession:CCMSLIB00004710288%26width%3D10.0%26height%3D6.0%26mz_min%3D%26mz_max%3D%26max_intensity%3D150.0%26grid%3Dtrue%26annotate_peaks%3D%5B%5B204.8952,284.0693,521.329%5D,%5B521.2615%5D%5D%26annotate_precision%3D4%26annotation_rotation%3D90%26cosine%3Dstandard%26fragment_mz_tolerance%3D0.2&sa=D&ust=1604063429168000&usg=AOvVaw0ECRKh1MCwlwrowwvMXBYK
Ectoine	219769	CCMSLIB0000218169	185.1012	https://www.google.com/url?q=https://metabolomics-usi.ucsd.edu/mirror?usi1%3Dmzspec:GNPS:TASK-124de327f32f474291a5037f41ac991d-spectra/specs_ms.mgf:scan:219769%26usi2%3Dmzspec:GNPS:GNPS-LIBRARY:accession:CCMSLIB00000218169%26width%3D10.0%26height%3D6.0%26mz_min%3D%26mz_max%3D%26max_intensity%3D150.0%26grid%3Dtrue%26annotate_peaks%3D%5B%5B125.0711,143.0816%5D,%5B143.1%5D%5D%26annotate_precision%3D4%26annotation_rotation%3D90%26cosine%3Dstandard%26fragment_mz_tolerance%3D0.2&sa=D&ust=1604063428992000&usg=AOvVaw2f3CK1d6FsQ3zgieEJNFYV

[Type here]

Chloramphenicol	111427	CCMSLIB0004710288	380.2794	https://www.google.com/url?q=https://metabolomics-usi.ucsd.edu/mirror?usi1%3Dmzspec:GNPS:TASK-124de327f32f474291a5037f41ac991d-spectra/specs_ms.mgf:scan:219769%26usi2%3Dmzspec:GNPS:GNPS-LIBRARY:accession:CCMSLIB00000218169%26width%3D10.0%26height%3D6.0%26mz_min%3D%26mz_max%3D%26max_intensity%3D150.0%26grid%3Dtrue%26annotate_peaks%3D%5B%5B125.0711,143.0816%5D,%5B143.1%5D%5D%26annotate_precision%3D4%26annotation_rotation%3D90%26cosine%3Dstandard%26fragment_mz_tolerance%3D0.2&sa=D&ust=1604063428992000&usg=AOvVaw2f3CK1d6FsQ3zgieEJNFYV
-----------------	--------	-------------------	----------	---

[Type here]

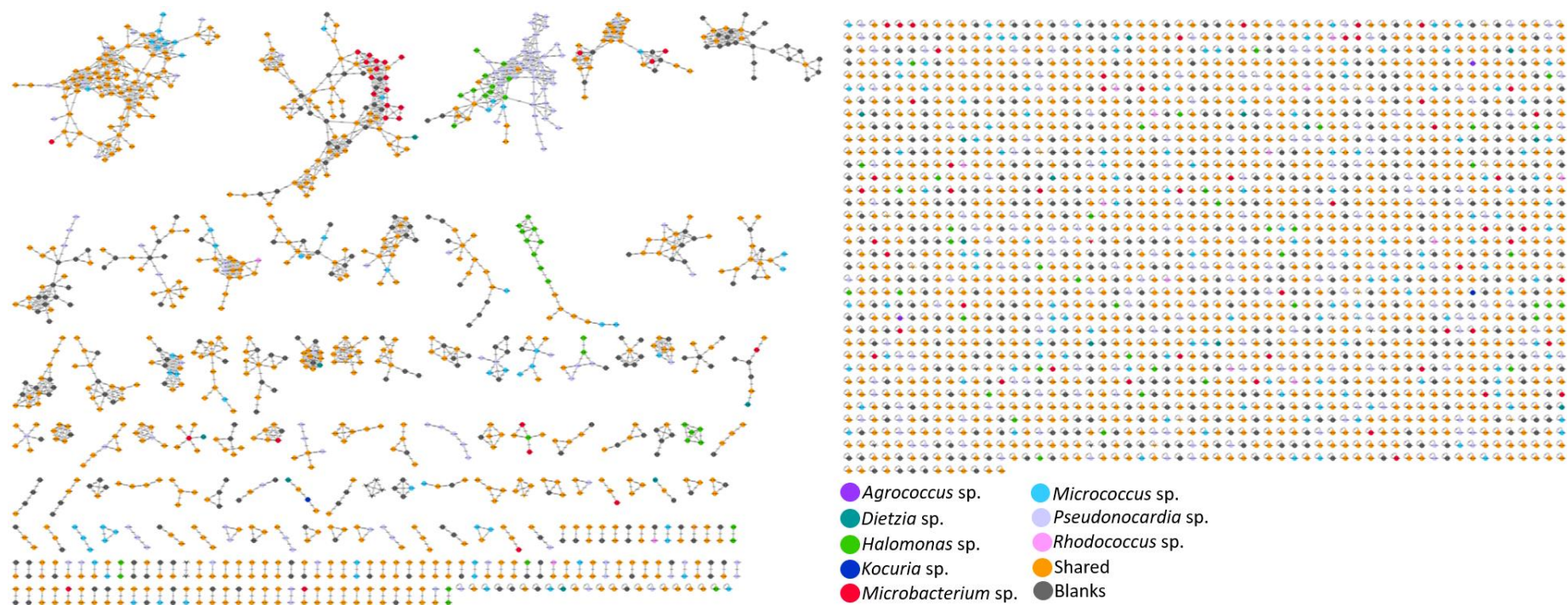


Figure S1: Molecular network of 3107 parent ions produced by 25 Polar actinomycete strains. Nodes are colour-coded based on genus: *Agroccoccus*, *Dietzia*, *Halomonas*, *Kocuria*, *Microbacterium*, *Micrococcus*, *Pseudonocardia* and *Rhodococcus*. Grey nodes represent media components whereas orange nodes represent parent ions that are produced by more than one different medium.

[Type here]

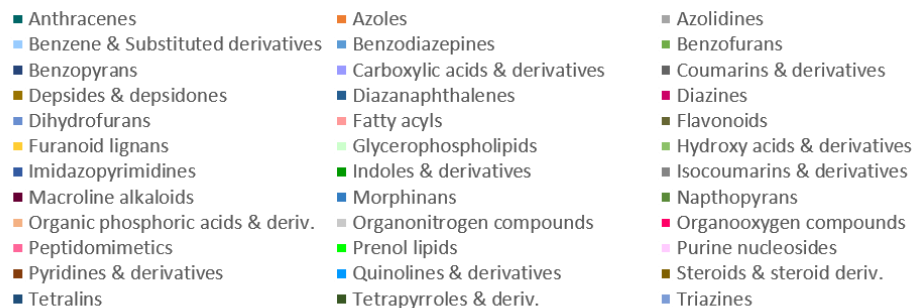
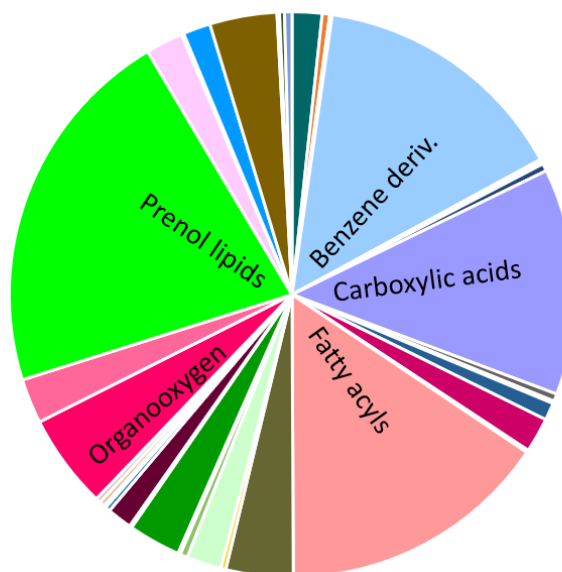


Figure S2: Pie chart showing the distribution of parent ions (%) between the 36 chemical class terms shown in the legend as annotated by MolNetEnhancer. The percentage of parent ions with no chemical class match (70.5%) is not shown in the pie chart. Each class has been colour coded to match the molecular network generated through MolNetEnhancer workflow analysis (Figure 5B)

[Type here]